Critical assessment of the MEDUSA gamma ray detection system for radon flux measurement on a tailings dam.

By

Tebogo Gladys Kgaugelo Motlhabane
B.Sc., University of North West
(2001)

A Thesis Submitted to the University of North West, in partial fulfilment of the requirements for the degree of Masters of Science in Applied Radiation Science and Technology

Supervisor: Dr. A.S. Tsela
(National Nuclear Regulator)

Examiner: Prof. E.J. Sendezera
(Physics Dept. University of Zululand)

Faculty of Agriculture, Science and Technology
Centre for Applied Radiation Science and Technology
University of North West (South Africa)

Mafikeng, 2003

I declare that this thesis is my own, unaided work. It is being submitted for the degree of Masters of Science in Applied Radiation Science and Technology in the University of North West, Mafikeng. It has not been submitted before for any degree or examination in any other University.

_____

_____ *Day of* _____ *2004*

ABSTRACT

Worldwide measurement of radon flux on mine tailing dams has been performed using various instruments. Some of the methods used in South Africa are electrets, alpha tracks, accumulator cans etc. Although these techniques and methods have been used for many years, a number of shortcomings are still evident. The major shortcomings are that, the methods lack spatial representivity that is, they only measure the radon flux at a point where they are placed and not the whole site in that way, the spatial variation is not shown in a site which is not homogeneous. Another shortcoming is that, they do not show seasonal variation and some have a back diffusion problem, and the time required for the result to be known is too long. For example it takes several days for electrets to gather sufficient information required, yet it is a single point result. This makes it difficult to steer the measurement. Furthermore, the moisture and atmospheric pressure on the mine dump influence some of the measurements.

The above shortcomings led to the investigation of a new technique based on gamma ray spectrometry to quantitatively assess the radon flux from the mine tailings dam. The system is called Multi Element Detector for Underwater Sediment Activity (MEDUSA). Initially, this technique was uniquely designed to measure the radioactivity on the sea floor where it proved to be successful. The major focus of this research study was, therefore, to critically assess the MEDUSA gamma ray detector system for measurement of radon flux on a tailings dam.

The process of determining the radon flux in this work involved field measurements using MEDUSA and laboratory measurements using Hyper Pure Germanium (HPGe) detector. The laboratory measurements were for correcting the field measurements. The HPGe has better advantage over MEDUSA in terms of resolution and this

means that the gamma ray energy peaks have better visibility than on the MEDUSA. The field measurements on the tailings dam were done using the MEDUSA mounted on a 4x4 vehicle, and simultaneously sample points were identified and samples collected.

The samples were measured for specific activity in the laboratory using gamma spectrometer with HPGe detector. These measurements enabled the determination of a factor that was used to calculate the activity of radium in the field. This activity was found to have an average of 309 $Bq.kg^{-1}$ with data range of 60 –540 $Bq.kg^{-1}$. A radon flux equation was then derived and used to calculate the radon flux on the field. Based on the radium content, the radon flux was calculated to average about $0.105 \pm 0.023\ Bq.m^{-2}.s^{-1}$

The results are within the same range as the previous flux measurement on the same tailings dam but with better statistics. This research work has demonstrated that the MEDUSA can be adapted for radon flux determination from tailings dam. The method promises to address some of the key shortcomings of existing techniques and the usefulness of this method can be extended to measuring radioactivity on contaminated sites for rehabilitation purposes.

Acknowledgements

I am very much grateful to the National Nuclear Regulator for giving me the opportunity to study by sponsoring me for this research project. I am also greatly indebted to the following people for making this research study possible,

- Dr. Alex Tsela, my supervisor, for the help in the preparations of this study and for taking me all the way until the end.
- Dr. Richard Newman, at IThemba LABS for his tireless support, motivation and being with me through every small detail of this study. I appreciated that, and will forever be grateful to you.
- Professor Robbie Lindsay and Professor Rob de Meijer both of University of the Western Cape for their expert opinions during the study, I would not have done anything without that.
- Mr. Zama Zituta, you took nothing and made it into something, your belief in the whole project and me is what took it to what it is now. Enkosi.
- Mr. John Pule of the NNR, and Gabriel Ntsume of Council for Geoscience, thank you for your contribution.
- Peane Maleka, Katse Maphoto, Dawid de Villiers and Lerato Sedumedi, my colleagues at iThemba LABS thank you for all your discussions that helped make this study a success. Le ka moso bagaetsho!
- My family, and friends for standing by and believing in me I love you.
- And most of all I would like to thank the Almighty for blessing me in everything I ever set my mind to.

TABLE OF CONTENTS

LIST OF FIGURES

LIST OF TABLES

Chapter 1

INTRODUCTION

1. Study motivation and background

Radioactivity is part of the environment we live in. Humans are exposed every day to radioactivity through the radioactive elements that occur naturally in the environment. Radioactivity is defined as the spontaneous disintegration of an unstable atomic nucleus and the emission of particles or electromagnetic radiation. The sources of this electromagnetic radiation, which are the naturally occurring radioactive elements, have been there ever since the earth was created. These elements occur in the form of decay chains. A decay chain is a series of transformations by a radioactive nuclide, which ends in a stable nuclide [34]. There are several decay chains that occur in nature. For this study, the important decay chains, which were focused on, were the ^{238}U, ^{232}Th and ^{40}K decay chains [see Figure 1]. Of these three, the most important one for this study is the ^{238}U series. The fifth member of this series is an element called radium, ^{226}Ra, which decays to give rise to the gas of the main focus in this study, radon, ^{222}Rn.

The disintegration of radium and release of radon eventually leads to the production of other decay products, which are ^{214}Bi, ^{218}Po, ^{214}Po and eventually the stable ^{206}Pb. Radon and its progeny are hazardous to human health and it was not until 1953 that this was understood [25]. Before that, houses were sometimes built with materials contaminated by the radium from uranium mines.

Radium is a metal that glows, and so it was also used in some instances to paint clock faces so that people could see the numbers glow in the dark. This action put people in contact with radium in danger of being irradiated. Radium is still sometimes

used to treat cancer, and it is also still occasionally used in luminous paints and vanishes. Radon was only identified as the gas coming from radium after 1898. [25]

There are human activities that contribute to an increase in the concentration of radon in the air. One such activity is mining which transfers uranium and radium from the deep mine to the surface in the form of waste sites where radon is exhaled, dispersed in the atmosphere and then breathed in by humans.

1.1 Radon – A Health Concern

In South Africa, uranium is sometimes produced as a by- product after the extraction of gold from the ore. Mining of gold involves crushing the gold bearing rock into a powder form, which is then taken through a chemical process in order to extract gold from the ore. Once the gold has been extracted, the waste, rich in uranium is stored in slimes dams. This slimes or tailings dam is a big mountain-like heap of rock and sand. It also contains dry, moist and wet areas, which could potentially exhibit varying radon exhalation or release rates. These areas are designated as edges, beaches and pond areas respectively, where the beach area encompasses the moister area between the wet pond and edge area of the slimes dam.

The South African gold mining industry is generally located in or near to major cities or towns and very often has substantial human settlements living in close proximity to the slimes dams. In some instances these settlements are mine villages or hostels housing mine employees or their families, while in other instances the settlements are made up of formal or informal townships housing the general public. [21]

Some of the above-mentioned communities are situated so close to the gold mine dumps that the closest houses are built on the slopes of the dumps. In other instances the closest houses are less than ten metres from the dump. [35]. This situation worries the nuclear regulatory authorities because of the resulting radiation exposure and hazardous health effects to these communities. This is also the reason why there are public hazard assessment reports required by the National Nuclear Regulator (NNR) from different mines. The NNR monitors the extent of radiation exposures by members of the public due to these mineral-processing activities. There are many ongoing studies of radon and its behaviour in order to find a better understanding of radon exposure to humans living near mines.

In these studies, the amount of radon released is measured using various devices, and techniques. Some of these techniques will be discussed in the chapters that follow. In this study, the focus was on exploring a new method of measuring the amount of radon produced on a tailings dam.

1.2 Problem statement

Radon is transported from the source (tailings dam) through the atmospheric or/and aquatic pathway to the members of the public living around or near the source. These people are referred to as the exposed group or loosely critical group. A critical group is defined as the group in a population, which is likely to receive the highest levels of radiation dose. [13]. Of the two pathways, the atmosphere is the most significant pathway through which radon will reach the public. This is due to the fact that radon is easily transported by air.

Lung cancer is the principal health concern associated with radon exposure. Radon itself being chemically inert does not accumulate to a great degree in the body. The

real problem lies in its short-lived decay products. Their deposition along the walls of various airways of the bronchial tree provides the main pathway for radiation exposure of the lungs. These decay products emit alpha particles and when they are breathed and deposited in the lungs, the alpha radiation can harm the secretory and basal cells of the upper airways and thus contributing to the increased risk of lung cancer. [28]. Some previous studies on radon exposed underground miners and externally irradiated atomic bomb survivors indicate that the human lung is sensitive to the carcinogenic effects of ionizing radiation. [10].

In trying to find some solution to the global radon problem, the focus of this project was put on radon exhalation from the source. There are several techniques and methods that have been used to quantify the amount of radon exhaled from the tailings dams. Some of them are, diffusion tubes, electrets, ionization chambers, scintillation cells, nuclear track detectors, activated charcoal detectors, closed box methods and others. The methods that have been used mostly in South African mine tailings by the radiation protection specialists for the purposes of public hazard assessments, are the diffusion tubes, the electrets, and the closed box methods. However, it has been known that the techniques have shortcomings or weaknesses regarding certain aspects:

(a) They fail to address spatial representivity

The instruments used to measure radon flux are small in size and when they are placed on a site where radon flux is measured they occupy a small space compared to total area of the site. On a non-homogeneous site, this means that the measured flux does not adequately represent the site's radon flux because the device samples a small portion of the site. The radon flux of a given area could not be represented by few measurements at few points of the measured site. Representivity is key to accurate characterization of the sources of radon.

(b) Seasonal variation

They are not designed to measure a distribution over various seasons.

(c) Back diffusion

Some of the radon measuring devices are inserted onto the ground, then radon gas diffuses through the soil and builds up inside the device. When this has happened, there will be pressure differential inside the device causing the radon to diffuse back into the soil. This does not give accurate measurement of the radon flux.

(d) Moisture content

Radon flux is greatly influenced by the moisture content of the environment.

(e) Measurements period

Many of the radon flux measuring devices require few hours to days of placement on a site to sufficiently capture enough data on radon flux. Also, because they are small, this means that for a whole area to be measured, different areas would have to be measured at different times depending on how many devices are available. The result is that a single tailings radon flux measurement could easily take a month or more. Such measurements take too long for a scientist or a mine company that needs to know radon flux within a short time and the public whose radiation dose needs to be known as a matter of urgency.

The above shortcomings led to the investigation of a new technique for measuring radon flux. This is the focus of this study. The method uses a mobile gamma ray detection system to quantitatively assess the radon flux from the mine dumps. The system is called **M**ulti **E**lement **D**etector for **U**nderwater **S**ediment **A**ctivity (MEDUSA). Therefore the main aim of the study is to critically assess the MEDUSA

Detection system for measuring the radon gas production on an old unused gold tailings dam.

1.3 Research Objectives

The objectives of this research were the following

- Acquiring skills in the use of the gamma ray spectrometry, in situ and in laboratory measurements.
- To determine whether the MEDUSA detector system could be used to measure radon flux on mine tailings.
- To make a comparative analysis with theoretical prediction of radon flux.
- To make a comparative analysis based on the results obtained through other techniques on the same tailings dam.

1.4 Justification

1.4.1 The study

- It is required that radon flux must be known in order to estimate exposure of people from radon. This study will help in the determination of levels of exposure due to radon received by the surrounding communities from the gold mine tailings.

- The methodology will either confirm the results obtained using other methods or indicate whether the methods used so far are over estimating or underestimating radon doses inhaled by the public from gold mine tailings. If it is found that these methods were underestimating the public doses, then NNR may need to consider further actions and recommend the use of MEDUSA methodology.

- For purposes of reporting to international committees like UNSCEAR, National Nuclear Regulator, NNR, must be confident that methods used to quantify doses were done using accurate methodologies.
- The study may show the need for re-examination of methods of measuring radon flux.

1.4.2 The technique

- It uses gamma ray spectrometry which is a widely used technique
- MEDUSA detector can cover a large area in a short time and . representative, real radon flux can be obtained in a short time.
- Allows for various detector crystals to be used.
- The change in activity concentrations relative to space can be quickly determined. Thus the radionuclide distribution for a given time can be reported. Therefore, by monitoring the place after some time, one can easily report any changes in radionuclide distribution and activity concentrations as a function of time.

1.5 Study Area

The study area (See Figure 2) chosen for this project was the Kloof Gold mine slimes dam number one. The reason this particular tailings was chosen is that, a study using a different technique was conducted on the same tailings. The idea was that the results obtained would be compared. Kloof gold mine is situated in Gauteng Province near a town of Westonaria. The study area, slimes dam number one is an old unused tailings dam. It has not been used in five years.

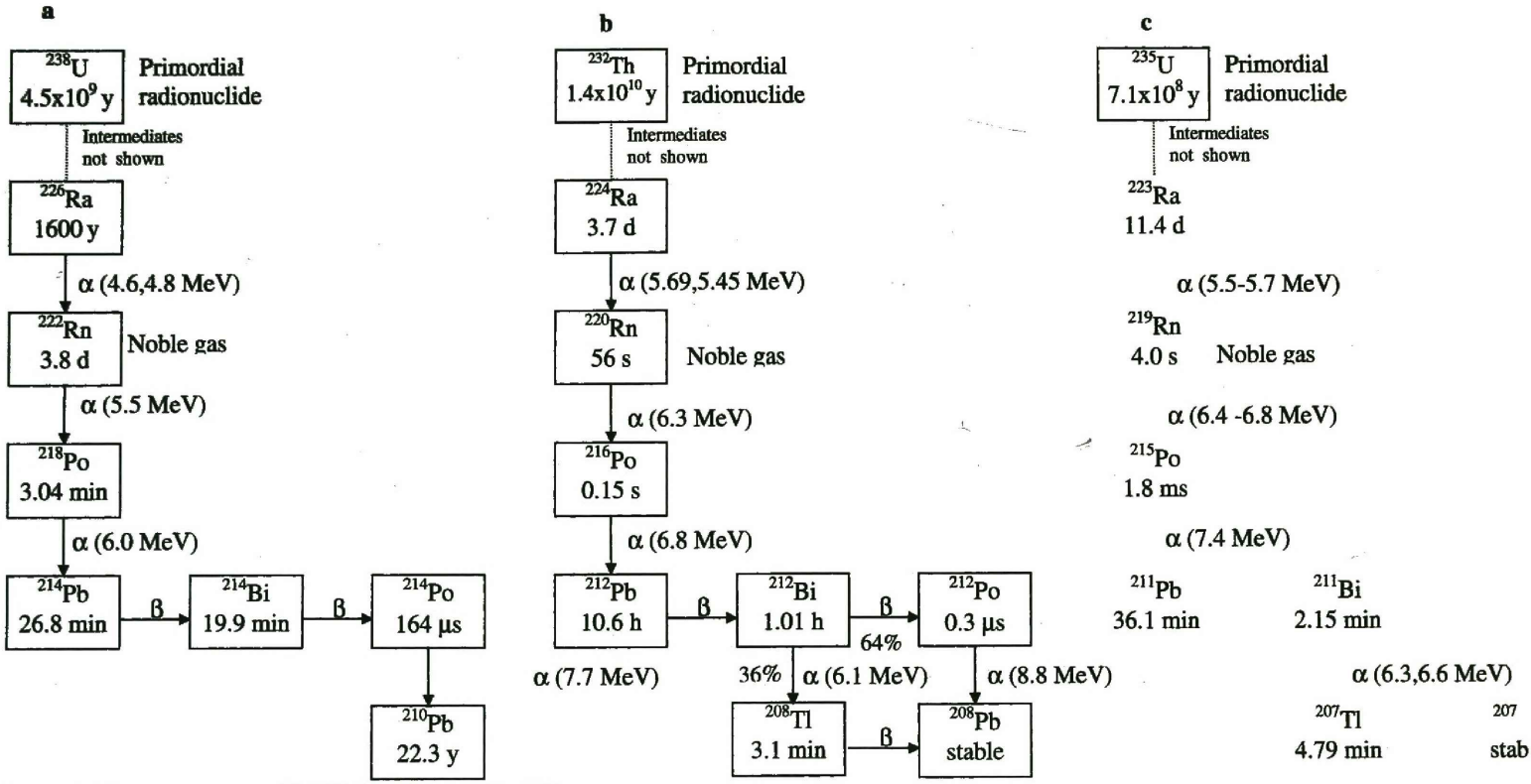

FIGURE 1: DECAY CHAINS OF U-238, TH-232 AND TH-234

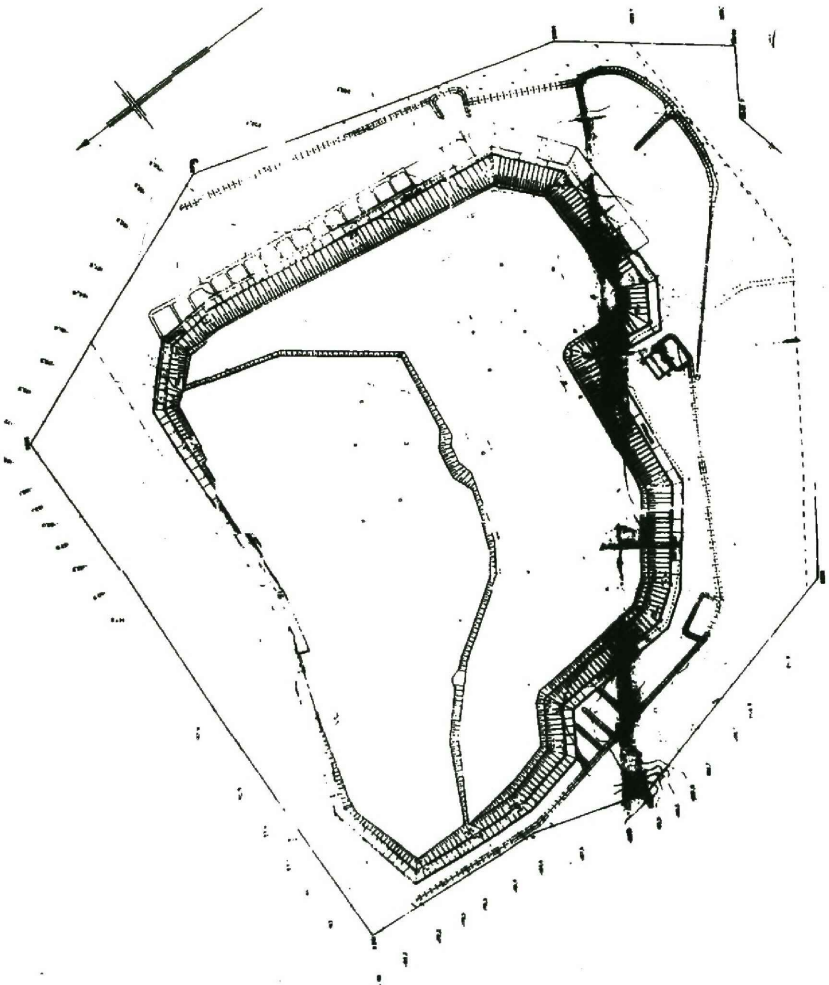

FIGURE 2: MAP OF KLOOF TAILINGS DAM NUMBER 1

1.6 Scope of the study

The study is mainly concerned with determining the relative amount of radon released from the mine tailings dam using the MEDUSA gamma ray detection system.

1.7 Thesis Outline

Chapter 1 introduces the study outlining the aims, justification and the problem statement.

Chapter 2 outlines the literature review on formation and movement of radon.

Chapter 3 discusses radon measurements and some techniques used in the industry.

Chapter 4 presents how the MEDUSA and HPGe detectors were set up for measurement.

Chapter 5 discusses the experimental setup and methodology used for the research study.

Chapter 6 presents the results found and their analysis and lastly

Chapter 7 gives summary, conclusions, recommendations and suggested future work that could be done.

Chapter 2

Formation and Movement of Radon - A literature review

2.1 Introduction

This chapter discusses how radon is produced and released into the surrounding environment. It also discusses the factors affecting the release of radon from the soil.

2.2 What is Radon?

Radon is a radioactive gas, which is invisible, tasteless, odourless and chemically inert. It is produced by the radioactive decay of the element, radium, ^{226}Ra. When radium decays to form radon gas, it loses two protons and two neutrons. These two protons and two neutrons form an alpha particle, which is a type of radiation. Radon also decays by losing an alpha particle to form the element Polonium.

There are three radioisotopes of Radon namely, ^{220}Rn also known as Thoron from the ^{232}Th decay series, ^{219}Rn also known as Actinon from the ^{235}U decay series and ^{222}Rn known as radon from ^{238}U decay series. The radioisotopes, Thoron and Actinon have half-lives of 55.6 seconds and 4 seconds respectively while ^{222}Rn has a half-life of 3.82 days. This results in the first two radioisotopes having more chances of decaying before escaping through the surface, because they do not have enough time to travel from their production site to the surrounding air while ^{222}Rn does. This escape is also made possible by the longer ^{222}Rn diffusion length (the average distance that an atom can move through dry soil before decaying.), which at 1.6 m is longer than ^{220}Rn, which is only 2 cm.

2.3 Radon Formation

The principal phenomenon that allows radon atoms to leave the grains of material in which it formed is the recoil of a nucleus due to alpha particle emission in the generation process of radon from radium. Each atom of radium decays by ejecting an alpha particle from its nucleus. During this process, kinetic energy, which is shared by the two atoms, is also released. A small fraction of the energy will cause the radon atom to recoil from the decay point and burrow through the grain while the alpha particle is ejected to the opposite direction. This recoil is the most important factor affecting the release of radon from mineral grains. [36;4]. This is represented by the following reaction:

$$^{226}_{88}\mathrm{Ra} \rightarrow {}^{222}_{86}\mathrm{Rn} + {}^{4}_{2}\mathrm{He} + 4.60\,\mathrm{MeV} \qquad \ldots \qquad 2.1$$

2.4 Radon Movement

Movement of radon in soil is complex, and has long been the subject of interest in the geochemical literature. It is governed by diffusion, convection and advection flow making it a challenge to predict what the radon concentration in the atmosphere is likely to be. [32].

Radon is transported from the soil in two steps, firstly emanation from the grain in which it is formed, and then secondly migration through the soil to the atmosphere and this is called exhalation.

2.4.1 Emanation

Emanation is the process that controls the movement of radon atoms from within solid grains into free intergrain spaces or pores of the soil. This process involves the radioactive decay of radium to radon within a grain and the subsequent escape of radon to the pore space. It is governed by the emanation coefficient, which is defined as the fraction of radon atoms generated within a solid (in this case a grain), which escapes from the solid. [25]. This emanation coefficient depends on the radium concentration, porosity, temperature, water content, and the radium distribution and the internal structure of the grain. [4]

Grain size and shape are two important factors that control the emanation of radon in soil. [28]. The location of the radium in the mineral grain i.e. how close it is to the surface of the grain, and the direction of the recoil of the radon atom i.e. whether it is toward the surface or the interior of the grain, determine whether or not the newly formed radon atom enters the pore space between mineral grains. If a radium atom is deep within a big grain, then regardless of the direction of recoil, it will not free the radon from the grain and the radon atom will remain embedded in the mineral. For a radon atom to escape from the mineral grain into the pore space, the decay must occur within the recoil distance of the grain surface. The range of recoil distance for ^{222}Rn is 20-70 nm in common minerals, 100 nm in water and 63 μm in air. [28]. For mineral grains with a typical density, a radon atom can leave the grain if its distance from an exterior surface is less than 0.07mm. [4].

Even when a radium atom is near the surface of a grain, the recoil may send the radon atom deeper into the mineral if the direction of recoil is toward the grains core. However, the recoil of some radon atoms near the surface of a grain is directed

toward the grain surface. When this happens, the newly formed radon leaves the mineral grain and enters the pore space between the grains.

After release of the radon atom from the parent grain, one of the following three mechanisms may take place,

1. If the pore space is filled with water, the range of the recoil radon atom is about 0.1 μm and the probability that it will be stopped by water is greatly increased. This increases the emanation coefficient.

2. If the pore is filled with air, the radon atom may be stopped in the pore air. This depends on how deeply embedded is the atom in the parent grain and the direction of the recoil.

3. If the recoiling atom has enough energy it may pass the pore air and get embedded into the adjacent grain. [19;24].

The above three mechanisms clearly show that the ability of a newly formed radon atom to become part of the soil gas depends on the grain size and the pore space moisture or water. Figure 3 gives a schematic representation of the above-mentioned three processes.

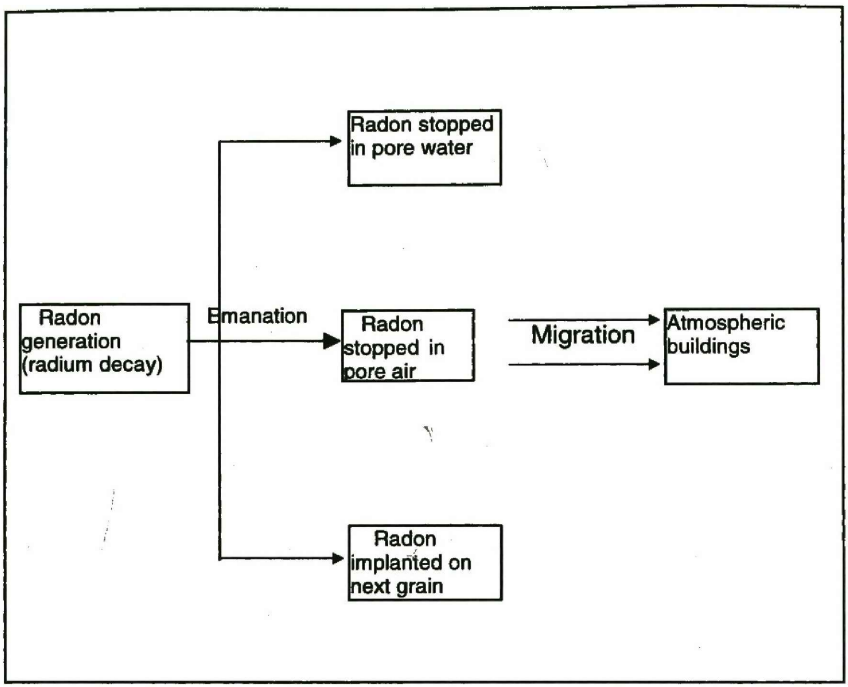

FIGURE 3:SCHEMATIC REPRESENTATION OF RADON EXHALATION, THE PRODUCTION OF RADON FROM WITHIN THE MINERAL GRAIN AND ITS SUBSEQUENT TRANSPORT INTO THE ATMOSPHERE.

Moisture content affecting emanation

Moisture content was found to have the greatest effect on the emanation coefficient for ores and tailings. [9]. This can be explained qualitatively by noting that the recoil range of radon in water is much lower than it is in air. Therefore the recoiling atom is most likely to be stopped by the water in the pore space instead of passing on to the neighboring grain. As more radon is stopped in the pore volume, there is an increase in radon atoms available for migration. This results in the emanation coefficient increasing with increasing moisture. However at moisture contents (up to about 5% by volume) few of the radon atoms can penetrate into adjacent particle and the emanation coefficient remains nearly constant with increasing moisture up to saturation.

2.4.2 Exhalation

Once the radon atoms are released into the pore spaces, they have to find their way into the atmosphere. These atoms are transported by diffusion and advection through the pore space until they decay or are released into the atmosphere.

This release into the atmosphere is known as exhalation. The exhalation rate, also known as the flux, is a measure of the liberation of radon from the surface of the tailings. The radon diffusion coefficient as well as the soil characteristics and the meteorological effects mainly characterize how much is exhaled. The diffusion coefficient relates the gradient of the radon concentration in air filled pores to the flux. [28].

Soil characteristics

The soil is characterized by factors like the soil's moisture content, porosity, permeability to gas movement, radium content and distribution. All these factors determine the emanation coefficient.

Moisture content affecting exhalation

The water in the pore space has a secondary effect on radon exhalation process. As the water content is increased the water starts creeping into cracks and surface imperfections of the grain and the soil become water logged. This has the effect of reducing the radon atoms that are able to diffuse into dead volume and hence the exhalation decreases as moisture increases. This is due to the reduced radon diffusion in water compared to air in the pore volume.

Permeability and porosity

Soil permeability is determined by the number, size, and degree of interconnection of pore spaces, which are controlled by the size, shape and arrangement of the soil grains. It is highest in coarse grained, well-sorted, spherical materials and lowest in poorly sorted and finer grained materials where smaller grains fill the void spaces between larger grains.

Radium content

Soils with higher radium content will tend to release more radon. Most of the radium atoms exposed to soil pore spaces stay attached to the grain surfaces or contained within grain coatings. The process of weathering moves radium atoms from within mineral grains where their liberated radon atoms will remain trapped within the grains, to sites on the periphery of grains where the liberated radon atoms will be available to pore spaces hence increasing the radon emanation coefficient of the soil.

Meteorological effects

These effects are changes in atmospheric pressure or temperature, or occurrence of precipitation. The exhalation rate increases when the atmospheric pressure decreases and falls when the pressure rises. This is because, high atmospheric pressure forces atmospheric air into the soil, diluting the near surface soil-gas and driving radon deeper into the soil. However, the long-term fluxes are not strongly dependent on atmospheric pressure changes. [9].

Long-term temperature changes may alter the flux. Research has found that increasing temperature caused an increase in radon exhalation. [18]. Higher

temperature slightly increases the value of the diffusion coefficient, which slightly increases the flux. [9]. Although the ambient temperature can fluctuate widely, the temperature within the tailings pile is more uniform. This means that the flux in the tailings pile is likely to stay the same at a uniform temperature.

This process of exhalation is mainly controlled by the amount of water present in the pore space, the percentage of pore space in the soil (porosity) and the interconnectedness of the pore spaces that determines the soil's ability to transmit water and air.

Chapter 3

Radon flux measurement

3.1 Introduction

In general, where more ^{238}U is found, more radon is expected. However, radon measurements are necessary to assess exposure from given tailings, because the actual concentration of radon in a structure is not easy to predict until measurements are made. Radon flux is measured as $Bq.m^{-2}. s^{-1}$. i.e. transfer rate per unit area of radon from the source or any solid substance to the atmosphere. Measurement of the exhalation rate is important in the study of radon exposure from soils.

The techniques that are used to measure radon depend on the radioactive properties of radon and its progeny instead of the physical properties. The radon products ^{218}Po and ^{214}Po emit alpha particles while ^{214}Pb and ^{214}Bi emit gamma particles. These products are then measured to determine the quantity of radon using various techniques. The beta particles can also be detected and counted, but they are much less penetrating than gamma rays and have lesser energy than alpha particles therefore they tend to be less sensitive indicators than alpha particles or gamma rays. [9].

There are also three modes of measurement of radon and the type selected depends on a number of factors including sensitivity, cost, convenience, and time available for sample collection and analysis. The types of modes are given below

Instantaneous mode

Here the radon concentration is determined over a short time and analyzed.

Semi- integrating (continuous mode)

The radon concentrations are allowed to reach a point where the rates of radon gas production are equal to the rate of decay. The device will later be sent for analysis.

Fully integrating time averaging

As long as the sampler or measurement device is exposed to radon it will continue to store information and after being removed it will maintain the information until it is analyzed. The sampling period could therefore vary from days to months. [9].

Different methods have been used for measurements of radon. These are divided into direct and indirect methods. Direct methods are those where the amount of radon is collected immediately using devices designed to do so and counted while the indirect methods involve determining the amount of radon through its progeny using gamma or alpha spectrometry.

3.2 Direct techniques

In measuring radon flux directly, the accumulation method is mostly used. Radon is accumulated in a container and a detector placed inside the accumulation box is used to measure the radon released. The detector measures the radon gas concentration. Some of the examples of the detectors used are the following

3.2.1 Electret system

Various mines measured the radon flux on the surface of mine dumps using the electrets. It is a flux monitoring system, which makes use of the principle of ionisation chambers. It consists of a charged Teflon disk (electret), open-faced ionization chamber, and electret voltage reader and data logger. When the electret is screwed into the chamber, a static electrostatic field is established and a passive ionization chamber is formed. When the ions are brought into such a chamber by the fast moving air flow through the alpha contaminated pipe, the negative ions are attracted to the charged surface of the electret which is positively charged, and the electret charge originally present gets reduced. The electret charge is measured before and after the exposure with a potable electret voltage reader, and the rate of charge is proportional to the radon flux.

The passive flux monitor consists of a 1*l* volume chamber with carbon coated Tyvek window with filtered vents. When it is positioned on the surface being tested, the radon from the ground enters the chamber through the window and exits through the vents. The semi-equilibrium radon concentration established inside the chamber is representative of dynamic radon flux from the surface. Because of the equilibrium between the surface and outside environment through the vents, the flux emanation from the surface is not disturbed. The electret discharge rate is a measure of the undisturbed radon flux. These flux monitors are calibrated by exposing them on well-characterised standard flux beds.

The advantage of these devices is that they (electret ion chambers) are inexpensive, simple, and passive with no moving parts or electronic components, unaffected by ambient environmental conditions and can be normally used for several measurements before a need for replacement of the electret. [33].

This system measures radon flux. Lower limit of detection is 0.24 pCi per m^2 per sec when measured over 8 hours and 0.08 pCi per m^2 per sec when measured over one day. It is still possible to measure lower values by measuring over a longer periods.

3.2.2 Alpha particle track detector

An alpha particle track detector is another example of a detector. The detector materials are bombarded by alpha particles producing narrow tracks on it. Chemical etching will then enlarge the tracks so that they can be counted using an ordinary optical microscope. First radon gas is allowed to diffuse into a container fitted with an alpha particle detector. The container is 100-300 mm and it is placed in a hole about 0.7 m deep. This allows gas in the container to equilibrate the soil gas at this depth. The radon concentration is then determined by alpha emission detected by an alpha particle track detector film.

The major disadvantage of the method is that the result is only valid for a short period time (<60 min). Another one is that, initially the concentration increases linearly but the rate of build up decrease due to back diffusion of the radon into the soil.

Other detectors, which could be used in the same way, are thermoluminiscence wafers; electronic solid-state detectors and Track etch cups.

3.2.3 Diffusion Tubes

Another technique that is used in South Africa to measure radon flux is the diffusion tube method. In the diffusion tube method the soil material from which radon flux is measured is compacted into tubes and sealed for fifteen days for secular equilibrium

to be reached. Then the tubes are opened and a radon gas monitor is inserted and the tube is sealed again for a further five days to measure the amount of radon concentration.

3.3 Indirect techniques

Radon has short-lived progeny (^{214}Bi and ^{214}Pb) and long-lived progeny (^{210}Pb and ^{210}Po). These can be determined in order to measure radon. The short-lived products are beta and gamma emitters and can be used to determine the amount of radon adsorbed on a material like charcoal. The long-lived progeny are usually measured on natural samples like rocks to determine the radon concentration to which they have been exposed to over the last 100 years.

3.3.1 Gamma ray spectrometry

Gamma ray spectrometry is a method that uses the gamma rays, which are photons, emitted by a radionuclide, to quantify the radionuclide's activity concentration. This is a result of the analysis of the energy spectrum of the gamma quanta emitted after beta or alpha decay of the radionuclides a gamma ray detector is used for the purpose of measuring gamma rays. Gamma rays are detected by means of the electrons they produce when they interact in the material of which the detector is made. The electrons produced by these interactions deposit their energies in the counter and then generate a voltage pulse that signifies the passage of the photon. The height of the voltage pulse is proportional to the energy deposited in the detector.

The main gamma ray interactions are photoelectric effect, Compton scattering, and pair production. [27;3;8]

Gamma ray scintillation detectors

The general description of a scintillator is a material that emits low-energy (usually in the visible range) photons when struck by a high-energy charged particle. When used as a gamma-ray detector, the scintillator does not directly detect the gamma rays. Instead, the gamma rays produce charged particles in the scintillator crystals, which interact with the crystal and emit photons.

Gamma-ray scintillators work on principle that, when radiation strikes a certain type of scintillation material, light is produced. This light then interacts with the photo cathode and electrons are emitted. The electrons are multiplied by about 10^6 by the dynodes in the photomultiplier tube. Then the anode collects the electrons and an electrical signal can then be measured. The light produced indicates the amount and energy of the original radiation. This material that emits light is called scintillation material.

From gamma to light

The detection process works like this, the gamma ray will interact with the scintillation material in one of the above-mentioned mechanisms i.e. photoelectric effect, Compton scattering or pair production to produce energetic electrons. The electrons will ionize some of the atoms in the material. When this happens, the electron ejected is not energetic enough to be a free electron i.e. it doesn't get raised to the conduction band therefore it will leave the original orbiting position but without leaving the atom. The energy of this electron (exciton) will be given to the activating material raising certain atoms to an excited state. These atoms will de-excite by emitting light. Materials used for scintillation are Sodium Iodide, Cesium Iodide, Calcium Fluoride,

and Bismuth Germanate. For this research study a Cesium Iodide detector crystal was used.

Semiconductor Detectors

According to the band structure model, the primary electrons produced by the gamma ray interaction raise secondary electrons to the conduction band leaving holes in the valence band. Semiconductors have their valence bands full and they have a limited degree of conductivity. The probability that an electron will be promoted to the conduction band is influenced by temperature. Cooling it reduces the number of electrons in the conduction band therefore reducing the background current and makes it much easier to detect the extra excitation due to gamma ray interactions.

There are two types of semiconductor detectors namely the Hyper Pure Germanium and Ge (Li) and they both share very similar operational properties. They are smaller than the Sodium Iodide detectors in volume and efficiency, but they have better energy resolution especially in analysis of complex gamma ray spectra and many closely spaced peaks. For this study, a hyper pure germanium detector was used.

3.4 Other Studies done

Gamma spectrometry has been used to measure radioactivity on majority of the studies [1]. In most cases it has not been used to measure radon flux on tailings dams. Most experiments to measure radon flux were performed using the above-mentioned techniques and other techniques.

The idea being used for this study, i.e. field measurements followed by samples being analyzed in the laboratory is not new. It has been used before by other scientists like [22; 17] to measure radioactivity. Field measurements in most experiments using gamma spectrometry were performed with a Sodium Iodide detector. The detector crystal used for this study was a Cesium Iodide crystal. Recorded values of the flux from surfaces of tailings dams range from 0.1 – 10 $Bq.m^{-2}.s^{-1}$.per $Bq.g^{-1}$ ^{226}Ra while the South African gold tailings have indicated values of less than 1 $Bq.m^{-2}.s^{-1}$. [13]

Chapter 4

Setup of MEDUSA and HPGe Detectors

4.1 Overview of MEDUSA detector system

MEDUSA is an acronym for **M**ulti **E**lement **D**etector for **U**nderwater **S**ediment **A**ctivity. The MEDUSA detector was developed through collaboration between Nuclear Geophysics Division of the Kernfysich Versneller Instituut in the Netherlands and the British Geological Survey. The design of the system is strongly influenced by the experience of the British Geological Survey with their Eel system.[30]. The system, like the name implies, was, and is still used for measuring radioactivity levels on the seafloor, and then characterizing sediments according to their radionuclide activity concentration. Although it was first meant for seafloor surveys, the MEDUSA can also be used in airborne surveys, land surveys (like in this study) and borehole experiments. [5].

The system uses a scintillation detector because it has an advantage over semiconductor detector in that it can be operated at higher temperatures. The scintillation detector crystal that had been used on sea floor surveys was Bismuth Germanate (BGO), but for this survey a Cesium Iodide, CsI (Na), crystal was used since it has better resolution. Figure 5 and 6. show the spectrum resolution results found using the CsI and BGO detectors. Furthermore, the light output for BGO crystal drops with increasing temperature compared to the CsI (Na)(See Figure 4).

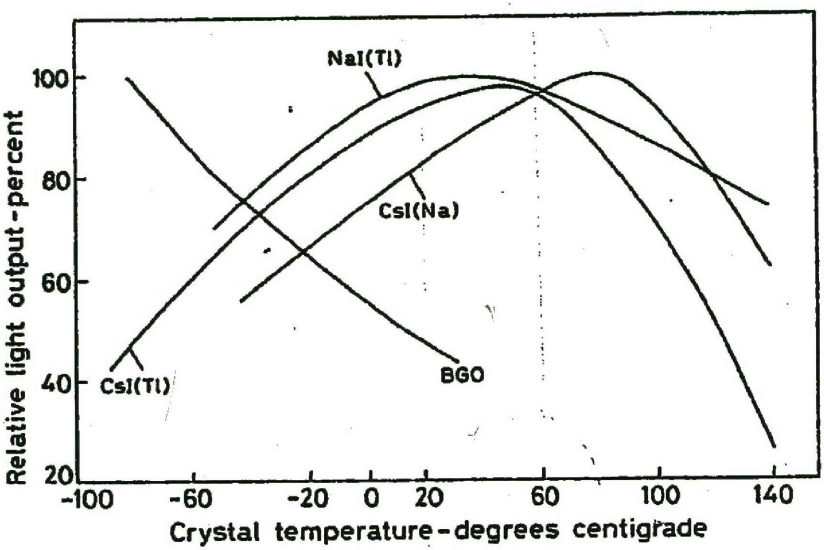

FIGURE 4: TEMPERATURE DEPENDENCE OF LIGHT OUTPUT FROM INORGANIC CRYSTALS.[2].

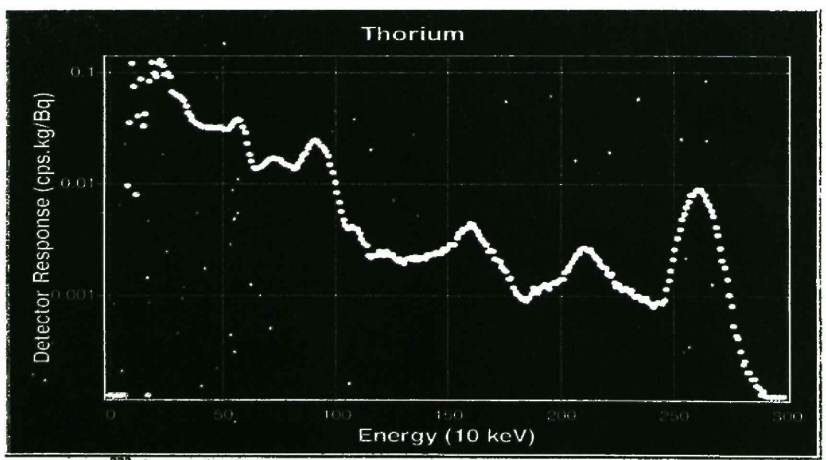

^{232}Th standard spectrum. Crystal type: 50x150mm cylindrical BGO

FIGURE 5:RESOLUTION ACQUIRED WITH A BGO CRYSTAL. NOTE: THE CRYSTAL DIMENSIONS ARE NOT THE SAME IN BOTH CASES I.E. FIG 5 AND FIG.6.[2]

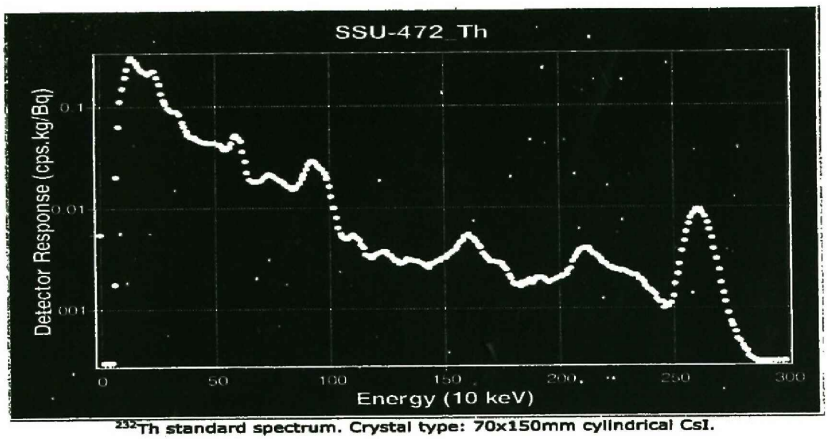

FIGURE 6:RESOLUTION ACQUIRED WITH CSI CRYSTAL. NOTE: THE CRYSTAL DIMENSIONS ARE NOT THE SAME IN BOTH CASES I.E. FIG 5 AND FIG.6.[2]

4.2 The Detector Components

The system is made up of two parts. The first part, which is enclosed in a 3mm thick stainless steel casing, consists of:

A CsI (Na) scintillation crystal of 70 mm diameter and 150 mm height and a resolution of less than 11% FWHM at 662 keV, and it is coupled to a photomultiplier tube. The photomultiplier tube converts light pulses supplied by the detector into voltage signal, the amplitude of which represents the amount of energy deposited in the detector. The photomultiplier tube has a 50 mm diameter.

The other components inside the stainless steel casing are the Cockroft Walton High Voltage generator, a pressure sensor and a telemetry board.

The second part of the detector system comprises an Aladdin box (see Figure 7) laptop computer, the Global Positioning System receiver, as well as MEDUSA software for data acquisition. The Aladdin box receives data from the detector and

sends command data and power down to the detector. The data it receives are energy spectra, pressure, sound, temperature and count rate.

The Global Positioning System, GPS, is a satellite navigation system. It provides specially coded satellite signals that can be processed in a GPS receiver, enabling the receiver to compute position, velocity and time. The device was interfaced to the laptop computer that was used to view the information provided by the detector.

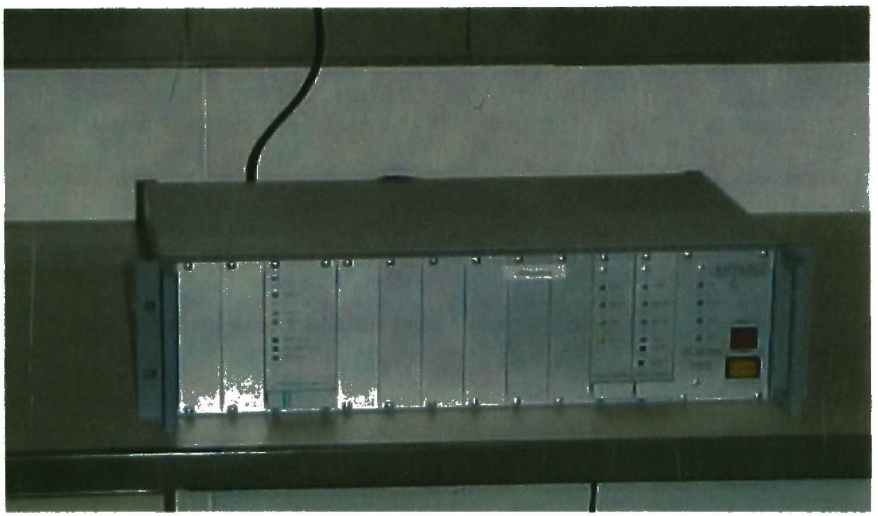

FIGURE 7: ALADDIN BOX.

4.3 MEDUSA Software

MEDUSA detector system uses Medusa Software for data acquisition and interpretation. The main program is called the MEDUSA Data Logger (MDL), and it is used for raw data collection. The other two are the MEDUSA Data Synchronizer (MDS), and MEDUSA Post Analysis (MPA). These two programs help in the manipulation and visualization of the data acquired by the MDL.

4.3.1 MEDUSA Data Logger

The MDL is a program where the plugins that are used to acquire and process data from the GPS, the detector and the Aladdin box, can be added. A plugin represents a piece of control software for a specific piece of hardware receiver. [31].

The spectral data were acquired using the Medusa Data Logger (MDL), which forms part of the MEDUSA software package, and the system was set such that a spectrum was acquired every five seconds while other data like the temperature, sound and counts were recorded every second. The time for acquisition of spectrum, five seconds, was for the area to be mapped with a reasonable spatial resolution. The raw data acquired were written to files stored on the laptop computer.

4.3.2 Synchronization of MEDUSA Data

The MEDUSA detector crystal temperature, the GPS determined co-ordinates, sound from the microphone, and the total detector count rate are read out every second, while a gamma ray spectrum is acquired every five seconds. In order to proceed with the determination of activity concentrations using the full spectrum analysis method it is necessary to make sure that there is a one to one correspondence between spectral data and other data types (these are: pressure, sound, temperature, total counts, altitude, latitude and time). This is achieved by means of the MEDUSA Data Synchronizer (MDS) program.

Since non-spectral data were acquired more frequently it was necessary to manipulate these data using one of the following operations: averaging over a 5 seconds interval, time averaging and selecting the last known values. Once the one

to one correspondence was achieved one could progress to using the MEDUSA Post Analysis package in the manner described below.

4.3.3 MEDUSA Post Analysis

After the data were synchronized (see discussion on MDS) the activity concentrations as a function of x and y co-ordinates on the tailings dam were determined using the Medusa Post Analysis (MPA) computer program which forms part of the Medusa Software Package. This program uses Full-spectrum Analysis (FSA) procedure to extract activity concentrations ($Bq.kg^{-1}$). The FSA procedure involves fitting a linear combination of standard spectra and a background spectrum to each measured spectrum.

The background spectrum used in this study was supplied with the MEDUSA software and was obtained from measurements conducted in river water. An example of the quality of fit obtained is shown in Figure 8, where the calculated best-fit spectrum is shown superimposed on the measured spectrum (acquired over a 5 s period). The activity concentrations extracted from the MPA were not expected to be accurate because the geometry of calibration (See section 4.4) was different from the measurement geometry.

To place these activities on an absolute scale, the normalization factors were determined by comparing the activity concentrations determined in the field with those calculated from radiometric measurements using HPGe. More detail on the normalization factors is given in chapter 6 of results.

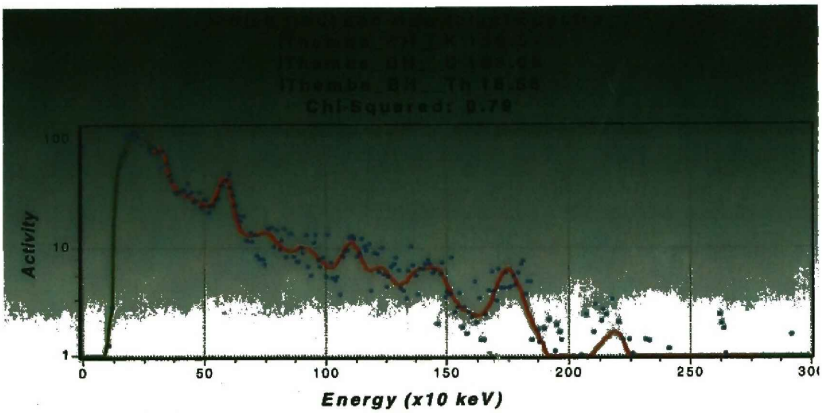

FIGURE 8: THE SOLID LINE REPRESENTS THE FITTED SPECTRA WHILE THE RAW SPECTRUM IS REPRESENTED BY THE DOTTED LINES.

4.4 MEDUSA Calibration

The calibration of MEDUSA was done in the Netherlands and consisted of the borehole mimicking calibration drums. Each of the drums contained well-known concentrations of ^{40}K, ^{238}U and ^{232}Th mixed with sand. The mixtures were in such a way that each drum had more of one radionuclide and the other two were lesser. Standard spectra were then obtained by measuring the response of a detector mounted inside the drums. These standard spectra represent the expected response of the MEDUSA detector to an activity of 1 $Bq.kg^{-1}$ of a particular nuclide. [20].

4.5 Mounting of the Detector

The System was mounted on a Toyota 4x4 that had a bull-bar in front. Steel brackets, which were specially designed for supporting the detector, were attached to the bull-bar. The detector was placed on the bulbar, 615 mm away from the ground and with the edge of the detector 453 mm away from the first part of the bracket. The second part of the system was placed at the back of the vehicle under the

canopy. Both parts were then connected with a cable that passed the power from the car battery via a DC to AC converter to the system. The antenna of the GPS was mounted on top of the canopy in order to receive signals easily. See Figure 9 and Figure 10 for the setup.

FIGURE 9: MEDUSA MOUNTED IN FRONT OF THE 4X4 VEHICLE THAT WAS USED ON THE SURVEY ON THE TAILINGS.

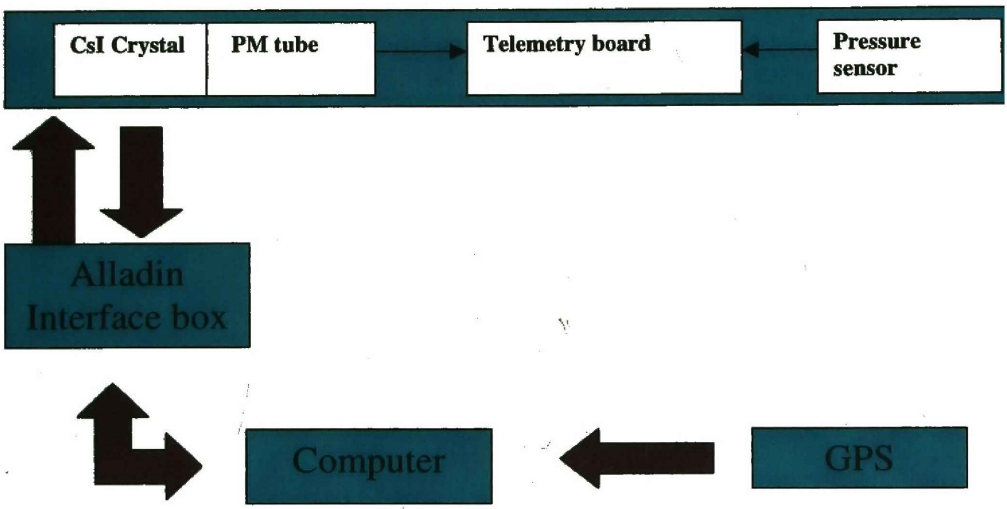

FIGURE 10: A SCHEMATIC REPRESENTATION OF THE MEDUSA SETUP.

4.6 HPGe Detector Setup

The HPGe detector at iThemba is a closed-end coaxial Canberra p-type detector, model GC4520 with built in preamplifier. It has a crystal diameter of 65.5 mm and it is 59.9 mm long. The detector is enclosed in an interlocking lead brick housing to ensure that the samples are measured under low background conditions. This lead shielding reduces the background from the cosmic radiation and from natural radioactive traces in the building. Lead is a choice of shielding because it has a high atomic number, it is cheap and also available. [8]. Without reduction, the background may exceed the activity from the sources and therefore the peaks of interest may not be visible. Data acquisition and analysis were performed using an OxfordWin-MCA program.

4.7 Energy calibration of the HPGe

Energy calibration was performed using a Europium, ^{152}Eu, standard source in order for peak position in the spectrum to be associated with certain gamma ray energy i.e. initially if the detector is not calibrated, the peaks are expressed as channels, after calibration they are expressed in energy (keV). [15;8]. Figure 11 shows a relationship between channels and energy.

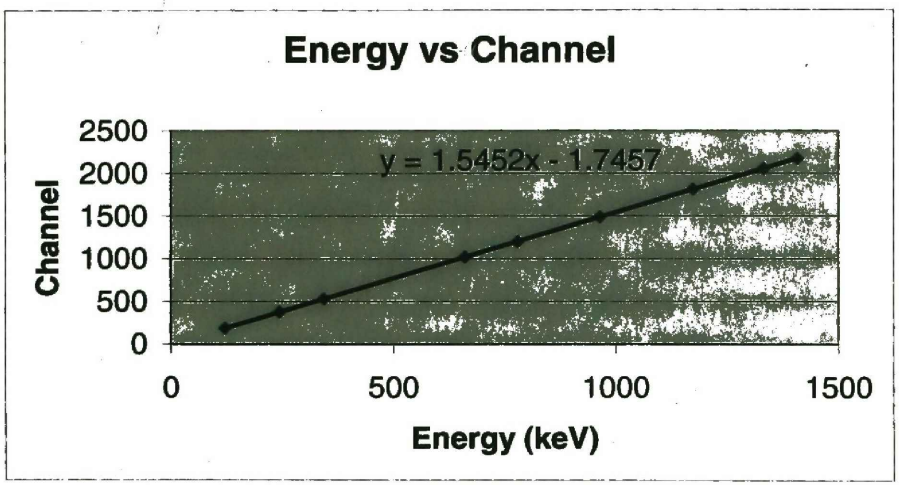

FIGURE11: ENERGY CALIBRATION.

4.8 Calibration of detection efficiency

The aim of the analysis is to measure the activity concentrations of ^{238}U, ^{232}Th and ^{40}K in sediment samples collected from the tailings dam. Activity is calculated using the following formula:

$$A = \frac{C}{LTxMx\varepsilon xBR} \qquad \text{.....4.1}$$

Where,

A, is the activity (Bq.kg^{-1}) ***Note****:Counts/second =Bq*

C, is the number of counts from the energy line of the measured radionuclide.

LT, is the live time for the acquisition of the spectra in seconds(s)

M,is the mass of the sample in kilograms (kg)

BR, is the branching ratio (dimensionless) and

ε, is the detector efficiency at a given energy (dimensionless)

All the above terms are readily available for calculation of activity except efficiency, which has to be calculated. Relative efficiencies associated with gamma ray energies of the uranium, thorium, and potassium were calculated, and later converted to absolute efficiencies. This then enabled the calculation of activities of ^{238}U, ^{40}K and ^{232}Th activities in the sample. In this method, Potassium Chloride, KCl, with the same geometry as the sample, was used for calibration instead of a standard source as usual. The procedure for the calculation of detector efficiency is discussed below.

1. First the spectra of the sample and of background using tap water were acquired; regions of interest were set through energies chosen in the thorium, uranium and potassium series. Real counts of the sample were determined by subtracting the background counts from the net counts of the sample and correcting for the time differences. This was done by using the following equation,

$$Ct = Cn - Cb(LTs / LTb) \qquad \text{.... 4.2}$$

Where,

C_t *is the total counts*

C_n *is the net counts of the sample*

C_b *is the net counts of the background*

LT_s *is the live time of the sample spectrum and*

LT_b *is the live time of the background*

The energies chosen for are the following:

TABLE 1:POTASSIUM ENERGY USED FOR EFFICIENCY CALIBRATION.

Radionuclide	***Energy (keV)***	***Branching Ratio***
^{40}K	*1461*	*0.107*

TABLE 2:URANIUM SERIES ENERGIES USED FOR EFFICIENCY CALIBRATION.

Radionuclide	***Energy (keV)***	***Branching Ratio***
^{226}Ra	*186*	*0.033*
^{214}Pb	*295*	*0.192*
^{214}Pb	*352*	*0.371*
^{214}Bi	*768*	*0.05*
^{214}Bi	*934*	*0.032*
^{214}Bi	*1120*	*0.15*
^{214}Bi	*1238*	*0.059*
^{214}Bi	*1377*	*0.04*
^{214}Bi	*1764*	*0.159*
^{214}Bi	*2204*	*0.05*

TABLE 3: THORIUM SERIES ENERGIES USED FOR EFFICIENCY CALIBRATION.

Radionuclide	***Energy (keV)***	***Branching Ratio***
^{228}Ac	*338*	*0.124*
^{212}Bi	*727*	*0.067*
^{228}Ac	*795*	*0.046*
^{208}Tl	*860*	*0.043*
^{228}Ac	*911*	*0.29*
^{228}Ac	*965*	*0.058*
^{228}Ac	*969*	*0.174*
^{228}Ac	*1588*	*0.036*

The branching ratios used are from Environmental Measurements Laboratory. [7]

2. An assumption was then made that the ^{238}U and ^{232}Th decay chains are in secular equilibrium and that the Uranium content was determined by the 352 keV energy line of ^{214}Pb (branching ratio percentage: 37.1%) and the thorium content was determined by the 338 keV energy line of ^{228}Ac(branching ratio percentage: 12.4%). Then the relative efficiency for each line in the Uranium series was determined by dividing $(C/Br)_E$ of each line by $(C/Br)_{352}$. For the Thorium energies the same was done but using the 338 keV energy line. This means that the relative efficiencies of the 352 keV and of 338 keV were assumed to be one. [15]. The examples of the curves for Uranium and Thorium relative efficiencies are shown on Figures 12 and 13 in the next page.

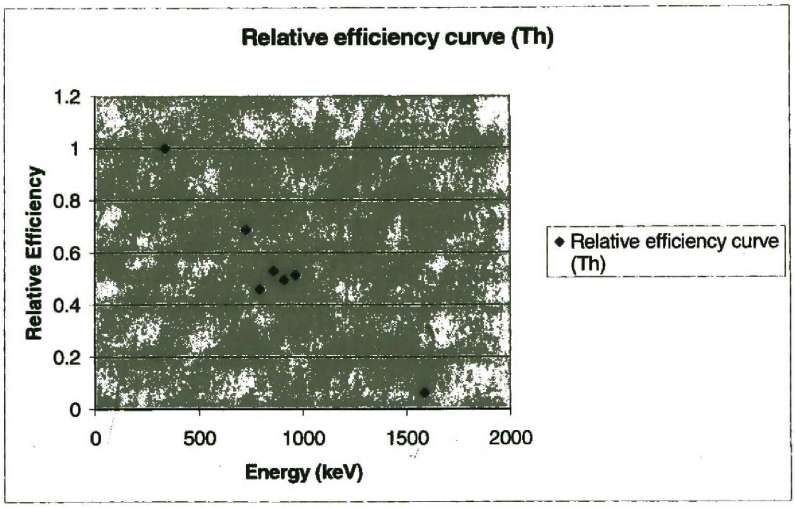

FIGURE 12: THE RELATIVE EFFICIENCY CURVE FOR THORIUM SERIES ENERGIES

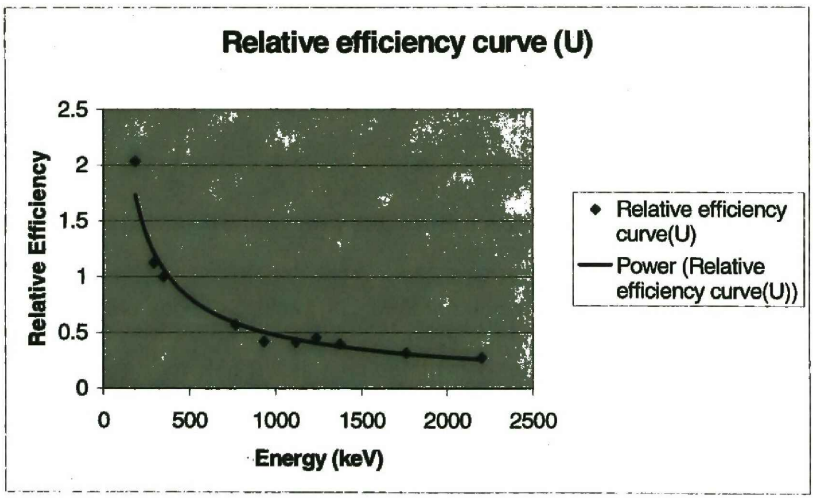

FIGURE 13: THE RELATIVE EFFICIENCY CURVE FOR URANIUM SERIES ENERGIES

3. Using the Uranium relative efficiencies, the fit parameters, a and b, were found through the equation,

$$y = c + mx \qquad \text{.....4.3}$$

$$ln\ \varepsilon_{rel} = ln\ a + b\ ln\ (E/E_0) \qquad \text{...4.3 (a)}$$

with E in MeV and E_0 = 1 MeV. These parameters were used to normalize the thorium data to the uranium relative efficiencies using the equation

$$\varepsilon_{rel} = a\ E^b \qquad 4.3(b)$$

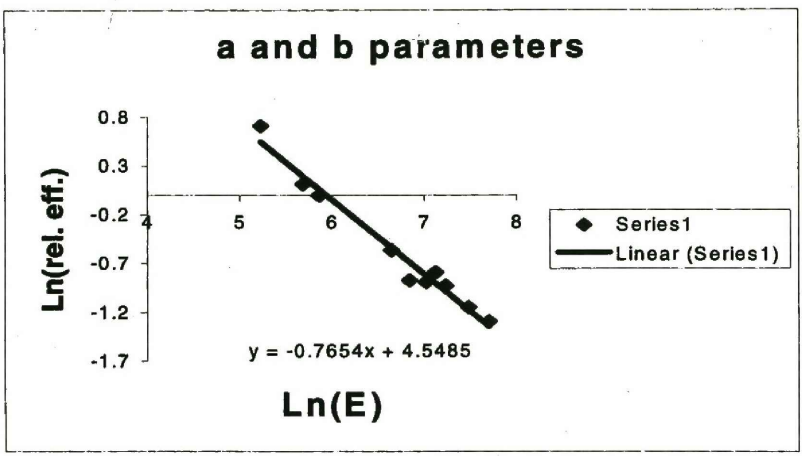

FIGURE 14: THIS DIAGRAM SHOWS HOW THE A AND B PARAMETERS WERE OBTAINED.

4. The ratio of the above acquired, ε_{rel}, from the above equation (in step 3) and the relative efficiency from step 2 was then determined for all the thorium values. The average of these ratios was then multiplied by the relative efficiencies in step 2. The values represent the normalized thorium relative efficiencies.

5. These values, together with the relative efficiencies of the uranium and the energy line 1461 keV of ^{40}K were used to find the second set of parameters, a' and b' which were used in equation 4.3(b), to find the final relative efficiencies of all the energies.

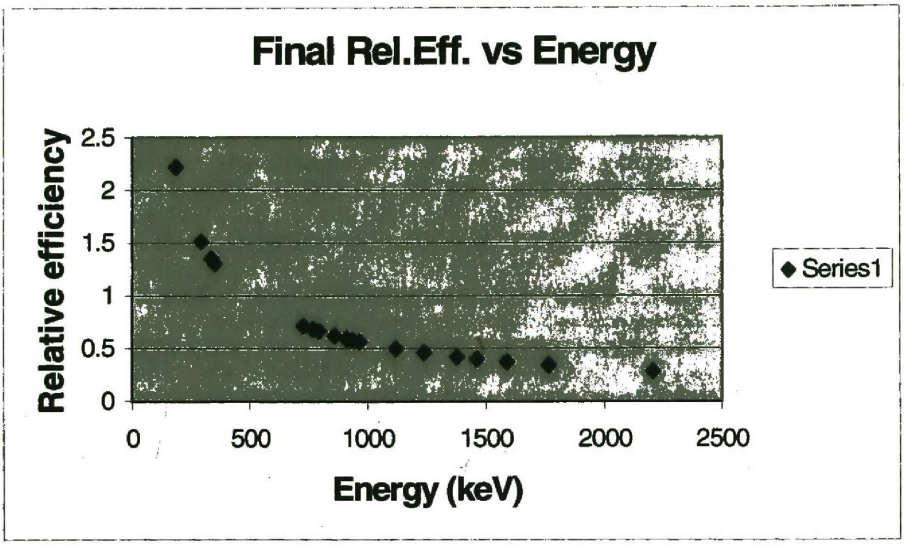

FIGURE15: A CURVE OF THE FINAL RELATIVE EFFICIENCY.

6. Now a sample of Potassium Chloride, KCl, with the same geometry as the soil samples was measured and its spectrum was acquired. Then absolute efficiency for detecting the 1461 keV line from ^{40}K was calculated. First the activity was calculated by using the equation,

$$A = \lambda N * \text{abundance} \qquad \ldots.4.4$$

Where,

A is the activity in $Bq.kg^{-1}$

λ Is the decay constant and λ = ln2/ half life of ^{40}K

abundance = 1.17×10^{-4}

N = number of moles x Avogadro's number

= n x 6.022×10^{23} (mol^{-1})

Equation 4.1 was then used to find the absolute efficiency

7. A ratio of the absolute efficiency of ^{40}K and the final relative efficiency of ^{40}K found in step 4 gave the coefficient, which was multiplied by the final relative efficiencies to give the absolute efficiencies. From this the activities of the various radionuclides could be calculated. The absolute efficiency as a function of gamma ray energy is shown in Figure 16.

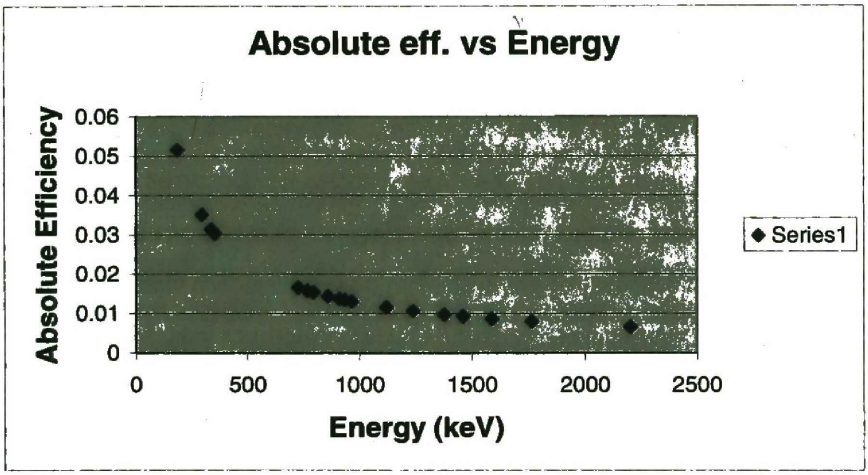

FIGURE 16: A CURVE SHOWING THE ABSOLUTE EFFICIENCIES OF ALL THE ENERGIES.

Chapter 5

Experimental Setup and Methodology

5.1 Introduction

This chapter discusses in detail the experimental procedures followed to measure the radon exhalation. The research study involved two parts of measurement, first field measurements where the MEDUSA detector system, a scintillation detector, was used and then laboratory measurements where the hyper pure germanium detector (HPGe) a semiconductor detector, was used. The field measurements took place on an old unused gold mine tailings dam where soil samples were also collected, while the laboratory radiometric measurements of the soil samples took place at iThemba LABS Environmental Radioactivity Laboratory. iThemba LABS is situated about 30 kilometers outside Cape Town. As will be shown in chapter 6 laboratory measurements were used to calibrate the field measurements. The two detectors were used because:

- The HPGe's energy resolution is much better than that of the Medusa detector.

- Using HPGe, the radon build up in the soil samples can be measured by using a Marinelli beaker, while with the MEDUSA detector it is not possible.

- The MEDUSA detector has a high detector efficiency, which allows measurement to be made in a relatively short time.

The field measurements were performed first. These data were used to select the sampling points. Below, the field measurements are discussed first, and then the laboratory measurements are described.

5.2 Field Measurements

The field measurements were performed at the Kloof gold mine's tailings dam outside Westonaria in the Gauteng Province, South Africa. The dam has not been in use for about five years. As a result it is dry. Vegetation was introduced on the dam surface in order to minimize soil erosion.

5.2.1 Field Measurement Procedure

The measurement started off first by choosing about 100 meters strip of land to be used for consistency checks, making sure that the detector was still in the right working order. This consistency check was also performed again by placing a Marinelli beaker full of Melkbos sand 23 cm away from the edge of the detector and measuring it for five minutes.

The next step then was to start measuring radon flux in the tailings dam. This was done by driving around the tailings on a 4x4 at speeds of about $2 m.s^{-1}$. Initially, the plan was to drive in at least 100 m x 100 m grids but this was not possible because of the following factors:

- The dam is partitioned into various sized divisions, which are differentiated by ridges. The presence of the ridges made it difficult to drive smoothly over the surface with a 4x4 vehicle. Some parts of the dam could therefore not be surveyed with the MEDUSA detector.

- After the use of the tailings dam was discontinued, lime, and then vegetation was introduced on the surface [11]. As a result some parts of the tailings were very difficult to be accessed with a 4x4 vehicle; therefore some areas were left as unmeasured gaps (see Figure 17). However, sediment samples were collected from these gaps for radiometric analysis in the laboratory. Consequently, the survey was conducted in zig-zag form and not along straight lines.

FIGURE 17: ONE OF THE DENSELY VEGETATED AREAS OF THE TAILINGS DAM.

5.2.2 Sample collection

The sample collection was done following a preliminary data analysis of the MEDUSA data. During data analysis, colour-coded maps of uranium, thorium, and potassium activity concentration were produced. From these maps the points from

which the samples were to be collected were identified. Sampling points were chosen on the basis of total counts and activity concentration and were chosen to represent a whole range of concentrations, that is, high, average and low counts. Table 4 shows the co-ordinates where the samples were collected in the field.

TABLE 4:SAMPLES IDENTIFICATION AND THEIR LOCATION.

Sample Code	***Coordinates***
Gap1	*S 26° 24.540' ; E 27 °37.351'*
Gap2	*S 26° 24.516' ;E 27° 36.870'*
Gap3	*S 26° 24.540' ;E 27° 37.038'*
Sample 6	*S 26° 24.785' ; E 27° 37.130'*
Sample 7	*S 26° 24.883' ; E 27° 37.257'*
Sample 8	*S 26° 24.522' ; E 27° 37.424'*
Sample 9	*S 26° 24.496' ; E 27° 37.370'*
Sample 10	*S 26° 24.388' ; E 27° 37.107'*
Sample 13	*S 26° 24.646' ; E 27° 37.291'*
Sample 14	*S 26° 24.410' ; E 27° 37.198'*
Sample 16	*S 26° 24.551'; E 27° 37.198'*
Sample 17	*S 26° 24.374' ; E 27° 36.915'*
Sample 19	*S 26° 24.621' ; E 27° 36.923'*
Sample 20	*S 26° 24.711' ; E 27° 37.012'*

5.3 Laboratory Measurements

The collected samples were taken to and measured with an HPGe detector at iThemba LABS Environmental Radioactivity Laboratory.

5.3.1 Laboratory measurement procedure

The measurement procedure consisted of sample preparation, energy and efficiency calibration, Background measurement, and sample measurement.

Sample Preparation

The soil samples were first sifted using a 2-mm sieve to remove the organic materials like grasses and roots and also to remove grains larger than 2 mm to attain homogeneity in terms of grain size. Then they were put into baking trays and dried overnight in an oven at a temperature of 110 °C. They were then put into Marinelli beakers and then weighed.

The samples were then sealed for them to attain secular equilibrium between radon and radium. Secular equilibrium means that the progeny have the same activity concentration as the parent nuclide. This means that if the activities of progeny radionuclides, ^{214}Bi, ^{214}Pb, are known, then that of the parent, ^{222}Rn is known. This is possible only if the gas in the uranium decay series, ^{222}Rn, does not escape. Sealing the sample container for radon to build up prevents this escape. The samples were sealed by first putting a copper disc over the sample in the Marinelli beaker and then applying a bath silicone along the edge of the disc to attach it and seal to the Marinelli beaker. The Marinelli beaker lid was placed on top and sealed as well.

Before the samples had reached 21 days required for ^{222}Rn to reach secular equilibrium they were measured once. After they reached 21 days they were measured again. They were not measured at a particular sequence of days, just randomly. They were each measured for 10 hours. The activities were then calculated using Microsoft Excel package.

Chapter 6

Results and data analysis

6.1 Introduction

This chapter presents the results and the analysis for the study. The results are followed by a discussion. The MEDUSA results are presented first followed by the HPGe detector results. A relationship between the two measurements is then shown. Also shown is how the radon flux calculation was done.

6.2 MEDUSA measurement results

MEDUSA results are presented in two forms. They are presented as a tri coloured maps representing the degree of activity concentrations of the radionuclides, uranium, thorium and potassium on the tailings dam. The colours are blue, red and yellow. The blue represents the lowest activity, yellow represents the average activity and the red colour represents the highest activity.

The other way in which the MEDUSA results are presented is in the form of frequency bar graphs. The reason for this is that the point-by-point activity concentrations could not be shown because the data would be too much to include in this document. The average and the standard deviation of the activities are also given. Both the average and the standard deviation were calculated using Microsoft excel package. They were calculated using equations below.

Calculation of the mean

$$Mean = \bar{x} = (1/n)\sum_{i=1}^{n} Xi \qquad \ldots 6.1$$

Where $X_{i,}$ is a set of measured values (i =1,2,3.... n) of quantity X

Calculation of the standard deviation

The standard deviation is a measure of how widely values are dispersed from the average value (the mean).

$$s = \sqrt{\frac{\sum (xi - \bar{x})^2}{n - 1}} \qquad \ldots 6.2$$

Where
$X_{i,}$ is a set of measured values (i =1,2,3.... n) of quantity X

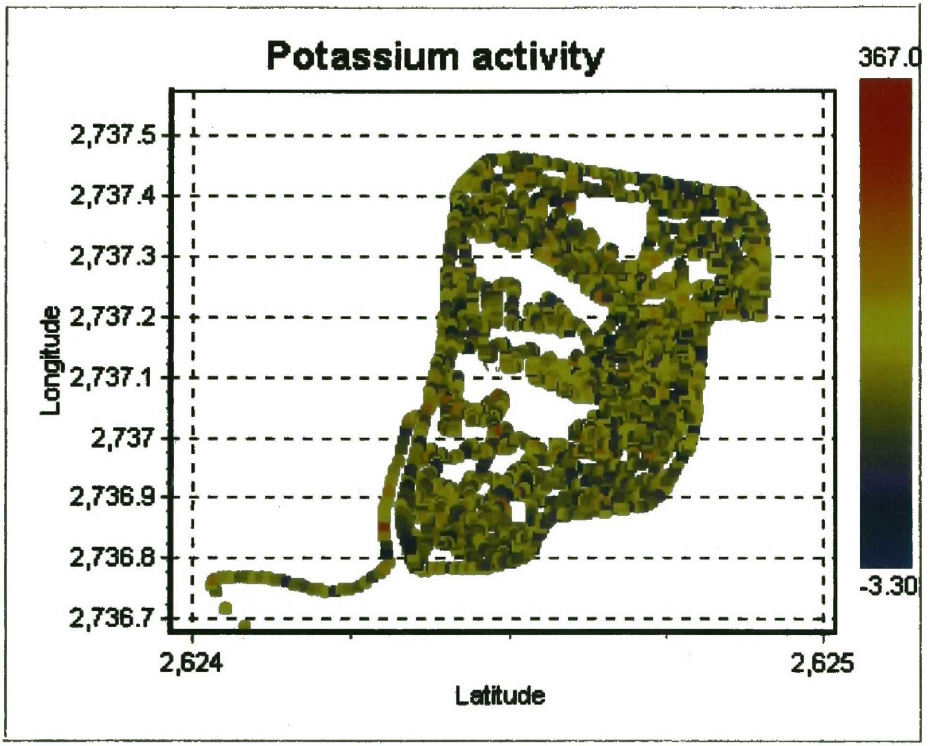

FIGURE 18: A MAP OF THE POTASSIUM ACTIVITY ON THE TAILINGS DAM.

The white areas are the gaps, which were not accessible. On the x-axis and the y-axis are the latitude and longitude co-ordinates respectively. The colour-coded bar on the right hand side, represents the activity concentration in $Bq.kg^{-1}$. The blue is lowest activity while the red colour represents the highest activity.

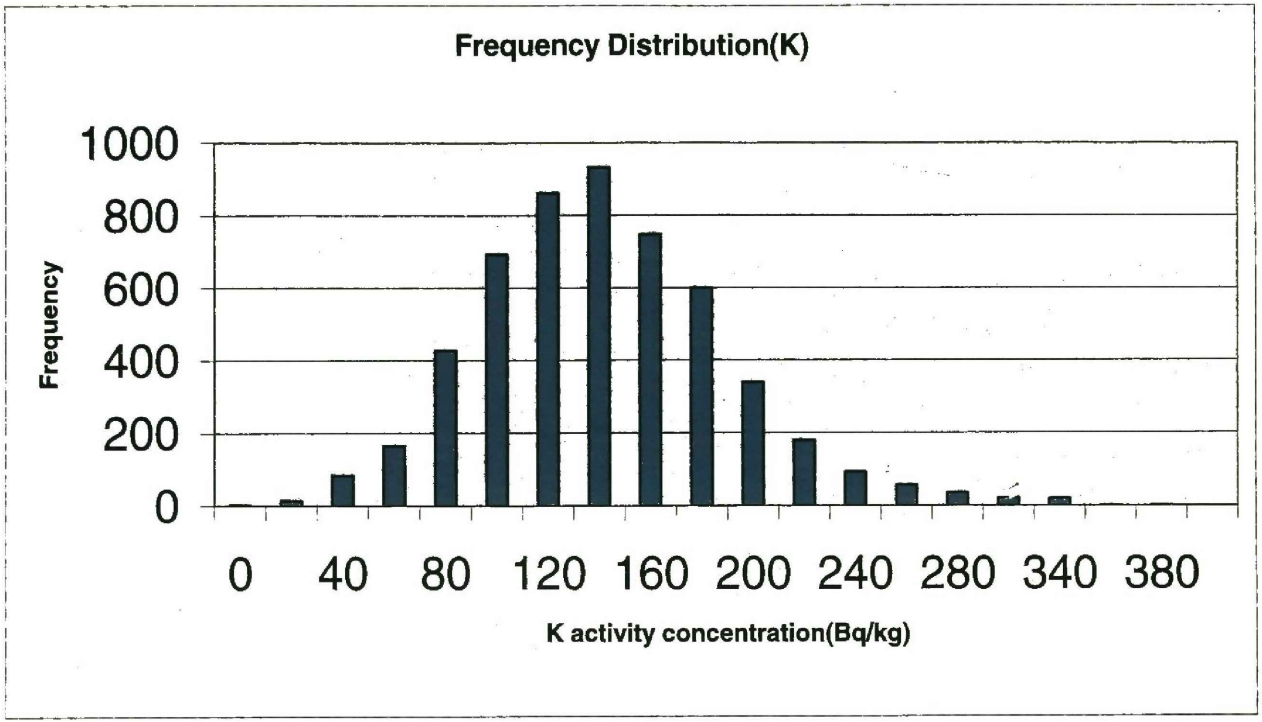

FIGURE 19: A REPRESENTATION OF THE POTASSIUM ACTIVITY CONCENTRATION FREQUENCY ON THE TAILINGS DAM.

TABLE 5:FREQUENCY DISTRIBUTION OF POTASSIUM ACTIVITY CONCENTRATION IN THE FIELD. ***Note: These activity concentrations are not yet normalized using radioanalytical analysis in the laboratory.***

Activity Conc. of K ($Bq.kg^{-1}$)	***Frequency***
0	*3*
20	*14*
40	*83*
60	*164*
80	*427*
100	*692*
120	*861*
140	*931*
160	*747*
180	*600*
200	*339*
220	*180*
240	*92*
260	*57*
280	*36*
300	*21*
340	*20*
360	*1*
380	*1*
400	*0*
Average =132.1± 48.3	

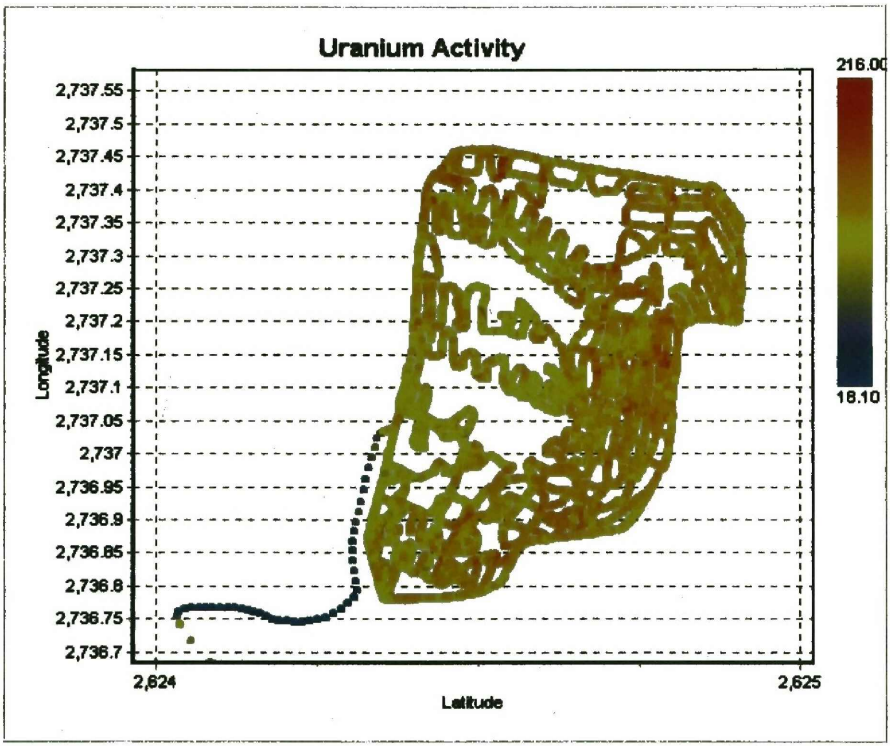

FIGURE 20: A MAP OF THE URANIUM ACTIVITY ON THE TAILINGS DAM.

The white areas are the gaps, which were inaccessible. On the x-axis and y-axis are the latitude and longitude co-ordinates. The color-coded bar on the right hand side represents the activity concentration in $Bq.kg^{-1}$. The blue is lowest activity while the red colour represents the highest activity.

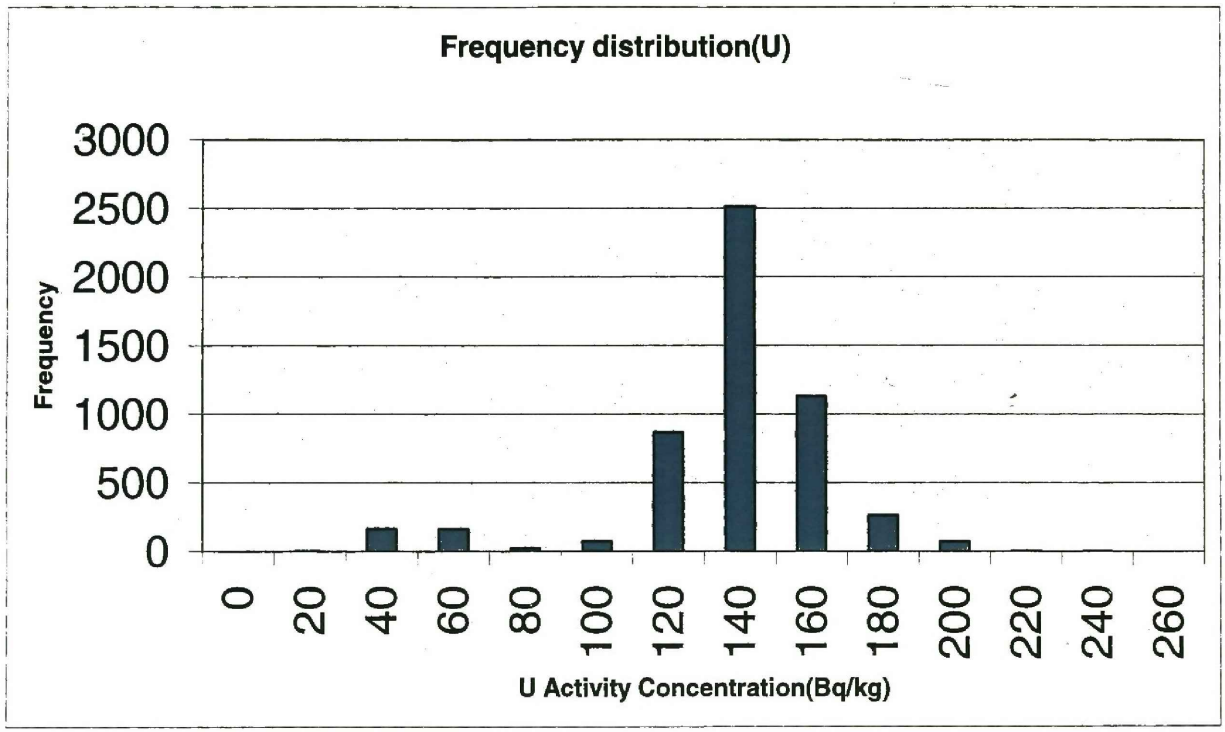

FIGURE 21:A REPRESENTATION OF THE URANIUM ACTIVITY CONCENTRATION FREQUENCY IN THE FIELD.

TABLE 6: FREQUENCY DISTRIBUTION OF THE URANIUM ACTIVITY CONCENTRATION IN THE FIELD. ***Note: These activity concentrations are not yet normalized using radioanalytical analysis in the laboratory.***

Activity Conc. of U (Bq/kg)	***Frequency***
0	0
20	2
40	163
60	162
80	22
100	74
120	867
140	2511
160	1130
180	263
200	71
220	3
240	1
260	0
280	0
Average = 128.0± 28.3	

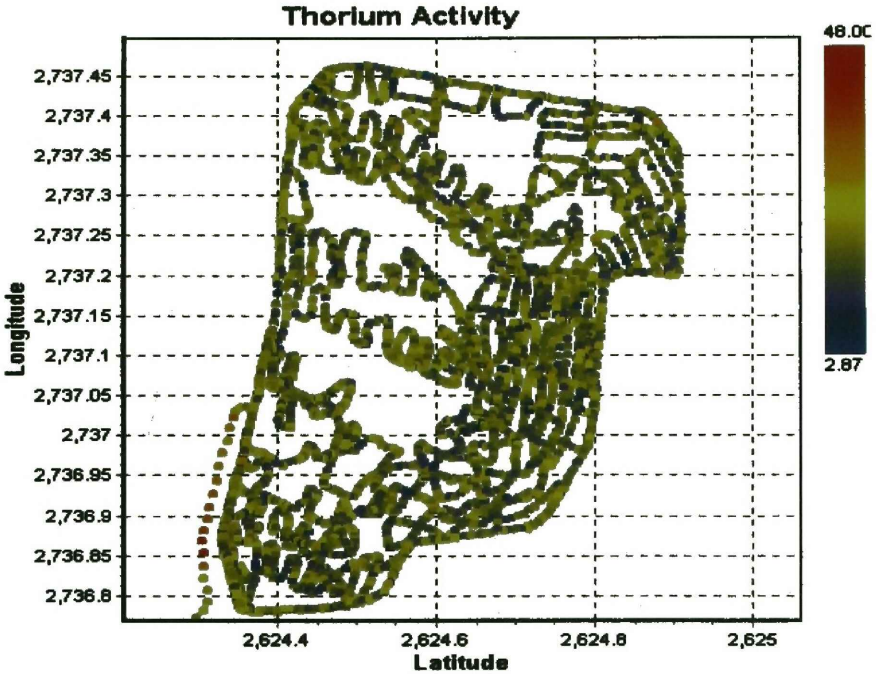

FIGURE 22: A MAP OF THE THORIUM ACTIVITY ON THE TAILINGS DAM.

The white areas are the gaps, which were inaccessible. On the x-axis and the y-axis are latitude and longitude co-ordinates. The colour-coded bar on the right hand side represents the activity concentration in $Bq.kg^{-1}$. The blue is lowest activity while the red colour represents the highest activity.

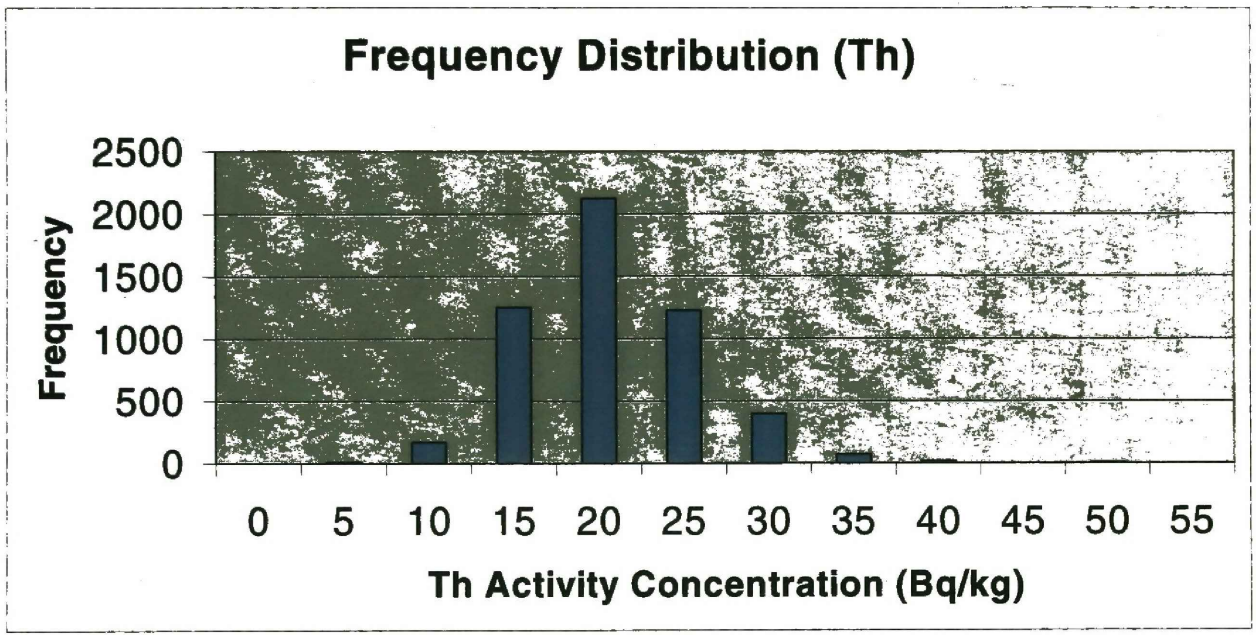

FIGURE 23: A REPRESENTATION OF THE THORIUM ACTIVITY CONCENTRATION FREQUENCY DISTRIBUTION IN THE FIELD.

TABLE 7:FREQUENCY DISTRIBUTION OF THE THORIUM ACTIVITY CONCENTRATION. ***Note: these activity concentrations are not yet normalized using radioanalytical analysis in the laboratory.***

Activity conc. of Th ($Bq.kg^{-1}$)	***Frequency***
0	*0*
5	*10*
10	*171*
15	*1250*
20	*2123*
25	*1225*
30	*400*
35	*71*
40	*15*
45	*0*
50	*4*
55	*0*
Average =18.2± 5.0	

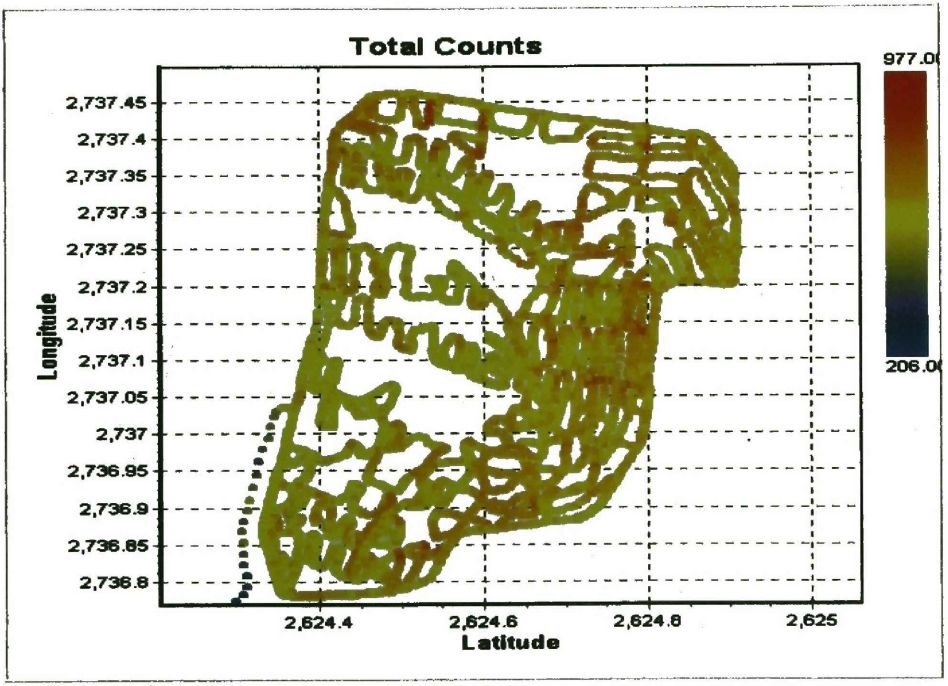

FIGURE 24:MAP OF THE TOTAL COUNTS.THESE COUNTS INCLUDE K-40,U-238 AND TH-234.

The white areas are the gaps, which were inaccessible. On the x-axis and y-axis are the latitude and longitude co-ordinates. The colour-coded bar on the right hand side represents the counts per second (Cnts/sec). The blue is lowest counts while the red colour represents the highest activity.

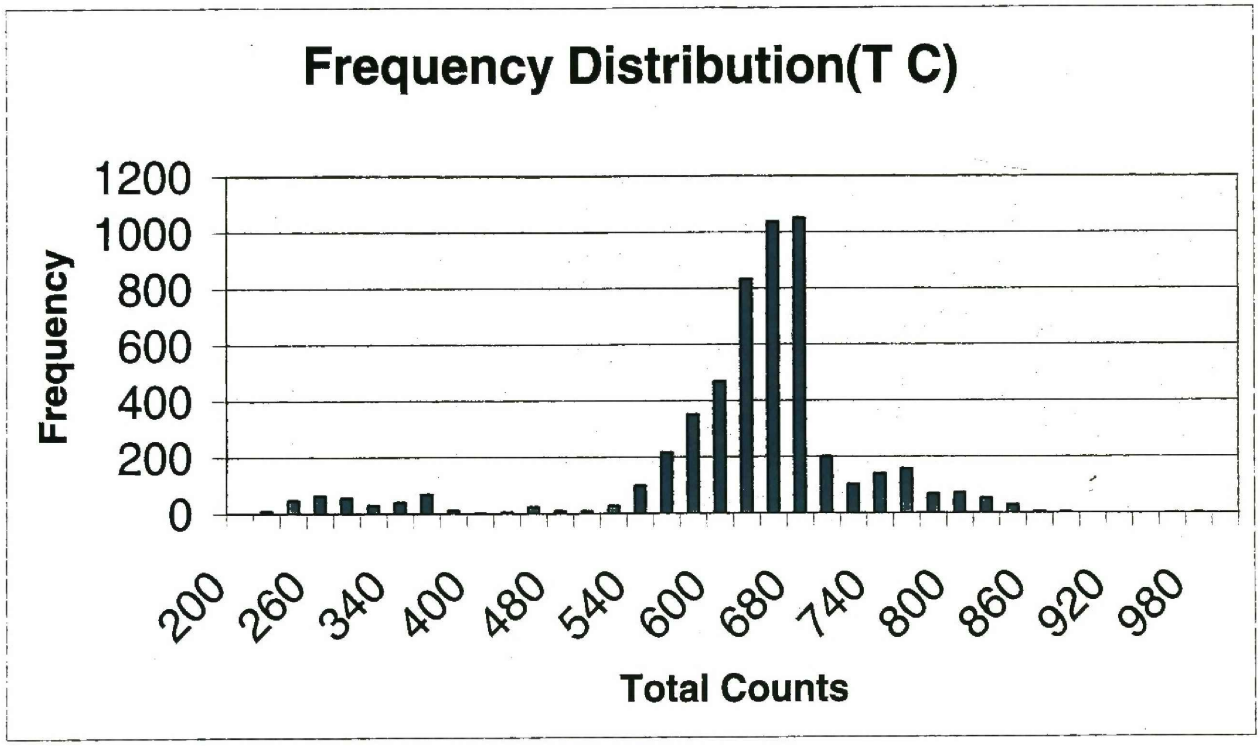

FIGURE 25:A REPRESENTATION OF THE TOTAL COUNTS FREQUENCY DISTRIBUTION IN THE FIELD

TABLE 8:FREQUENCY DISTRIBUTION OF TOTAL COUNTS IN THE FIELD.

Total Counts	Frequency
200	0
220	9
240	47
260	63
280	55
300	29
340	40
360	68
380	12
400	1
420	5
460	23
480	9
500	9
520	27
540	98
560	215
580	351
600	467
620	832
640	1036
680	1049
700	200
720	102
740	132
760	156
780	67
800	72
820	52

840	27
860	5
880	3
900	0
920	0
940	0
960	1
980	1
1000	0
Average= **614.1 ± 103.0**	

6.3 The Laboratory (HPGe) Measurements

The following are the results of the laboratory measurements. They are the weighted averages of the Uranium, Thorium and Potassium activities with uncertainties before 21 days had passed. The sample code is in no particular order. Gap 1, 2, 3 represent the sample points where the 4x4 vehicle could not access.

TABLE 9: LABORATORY RESULTS MEASURED BEFORE 21 DAYS.

Sample code	*Uranium*	*Thorium*	*Potassium*
Gap 1	*245.01± 8.93*	*16.31± 1.1 3*	*235.04± 4.06*
Gap 2	*270.62± 11.00*	*17.20± 1.43*	*246.98± 6.19*
Gap 3	*176.42± 7.91*	*12.94± 6.09*	*216.21± 3.40*
Sample 6	*301.44± 11.97*	*19.26± 0.96*	*254.16± 4.59*
Sample 7	*263.94± 27.88*	*15.95± 2.82*	*237.79± 65.14*
Sample 8	*258.45± 8.37*	*18.17± 0.99*	*217.16± 4.72*
Sample 9	*299.09± 7.47*	*18.72± 1.57*	*286.77± 5.18*
Sample10	*303.75± 9.60*	*20.26± 1.43*	*269.67± 9.78*
Sample 13	*263.48± 8.62*	*16.79± 1.81*	*242.22± 4.87*
Sample 14	*259.46± 6.81*	*18.38± 0.86*	*216.24± 9.14*
Sample 16	*190.80± 5.91*	*15.46± 0.69*	*202.66± 6.98*
Sample 17	*249.26± 8.81*	*14.64± 1.39*	*246.61± 5.44*
Sample 19	*299.96± 10.23*	*17.88± 0.97*	*215.10± 4.85*
Sample 20	*233.89± 5.65*	*17.01± 0.58*	*197.00± 3.20*
Average	*258.25± 37.47*	*17.07± 1.87*	*234.54± 24.63*

These are the weighted averages of the Uranium, Thorium and Potassium after 21 days had passed in the laboratory.

TABLE 10: LABORATORY RESULTS MEASURED AFTER 21 DAYS.

Sample Code	*Uranium ($Bq.kg^{-1}$)*	*Thorium ($Bq.kg^{-1}$)*	*Potassium ($Bq.kg^{-1}$)*
Gap 1	*284.± 0.22*	*18.07± 2.16*	*232.63± 4.49*
Gap 2	*281.24± 9.73*	*18.98± 0.95*	*247.79± 4.26*
Gap 3	*221.29± 5.50*	*16.61± 1.61*	*215.65± 11.89*
Sample 6	*313.54± 7.12*	*20.78± 0.32*	*247.30± 4.92*
Sample 7	*262.38± 11.25*	*16.65± 1.13*	*236.53± 6.47*
Sample 8	*263.46± 12.00*	*15.53± 1.21*	*210.69± 6.21*
Sample 9	*316.08± 13.74*	*19.43± 1.67*	*275.45± 6.97*
Sample 10	*329.10± 7.97*	*19.85± 1.08*	*264.97± 5.48*
Sample 13	*288.25± 10.46*	*21.20± 1.36*	*241.28± 11.53*
Sample 14	*249.37± 6.47*	*17.38± 0.81*	*204.91± 8.71*
Sample 16	*153.03± 5.54*	*14.05± 0.77*	*199.89± 3.54*
Sample 17	*265.50± 6.98*	*18.88± 1.24*	*244.58± 13.95*
Sample 19	*298.41± 12.06*	*16.36± 1.34*	*211.11± 6.84*
Sample 20	*262.84± 6.87*	*14.72± 1.10*	*201.77± 12.69*
Average	*270.60± 44.39*	*17.75± 2.21*	*231.04± 24.09*

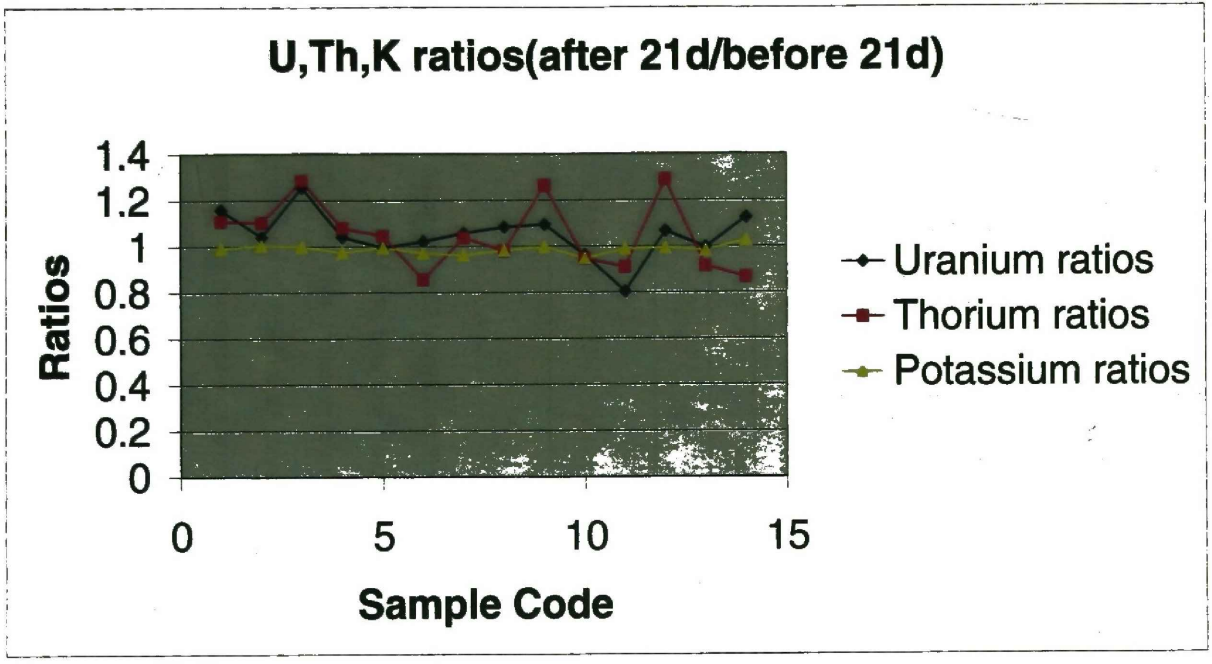

FIGURE 26: A PRESENTATION OF THE RATIOS OF THE THREE RADIONUCLIDES BEFORE AND AFTER 21 DAYS HAD PASSED.

TABLE 13:URANIUM, THORIUM AND POTASSIUM LABORATORY RATIOS BEFORE AND AFTER 21 DAYS

Sample Code	Uranium	Thorium	Potassium
Gap 1	1.16	1.11	0.99
Gap 2	1.04	1.10	1.00
Gap 3	1.25	1.28	1.00
Sample 6	1.04	1.08	0.97
Sample 7	0.99	1.04	0.99
Sample 8	1.02	0.85	0.97
Sample 9	1.06	1.04	0.96
Sample10	1.08	0.98	0.98
Sample 13	1.09	1.26	1.00
Sample 14	0.96	0.95	0.95
Sample 16	0.80	0.91	0.99
Sample 17	1.07	1.29	0.99
Sample 19	0.99	0.92	0.98
Sample 20	1.12	0.86	1.02
Average	**1.05± 0.10**	**1.05± 0.15**	**0.99± 0.02**

The measurements taken before 21 days and those after 21 days have a difference on average of about 5% for the Uranium results. This is negligible considering experimental uncertainties. This indicates that secular equilibrium was almost reached during the measurement before 21 days; therefore the wait for 21 days is not absolutely necessary since the difference is almost negligible.

6.4 MEDUSA and HPGe results: A synthesis

Table 11 presents the activity concentrations as given out by the MEDUSA in the field at selected sample points. A ratio of field and laboratory results for the three radionuclides (U, Th and K) determines the conversion factors through which the field activities (as determined from the MPA analysis) were converted onto an absolute scale. During the field measurement however, the location where sample 6 was picked up, was measured for about twenty minutes unlike other points, which were measured while driving. This makes this point's measurement the most accurate of all the sample points therefore; its ratios were used to normalize the field measurements instead of the average ratio of all the points being used. The conversion factors were calculated as ratios of laboratory (after 21 days had passed) and field results as shown in equation 6.3:

$$\textit{Conversion Factor} = \frac{\textit{Laboratory activity concentration}}{\textit{Field activity concentration}} \qquad \ldots 6.3$$

$$\textit{Absolute field activity conc.} = \textit{MFA X conversion factor} \qquad \ldots 6.4$$

Where the MFA is the field activity obtained through MEDUSA

The uranium values in the field are actually the measurement from the ^{238}Uranium progeny and these can be used to calculate the concentration of the ^{226}Radium in the field. Table 11 shows field results as measured by MEDUSA where the samples were picked, the laboratory results for the same points as measured by HPGe are shown in table 9 above. Table 12 then presents the laboratory to field ratios as calculated using equation 6.3

TABLE 12:FIELD RESULTS OBTAINED THROUGH THE MEDUSA AT SELECTED LOCATIONS.

Sample code	Uranium	Thorium	Potassium
Gap 1	INACCESSIBLE AREA		
Gap 2	INACCESSIBLE AREA		
Gap 3	INACCESSIBLE AREA		
Sample 6	130±7	18±4	125±42
Sample 7	140±7	12±4	153±42
Sample 8	128±7	20±4	143±42
Sample 9	121±7	18±5	104±40
Sample10	119±7	17±5	99±37
Sample 13	123±7	18±5	152±42
Sample 14	166±7	13±5	117±41
Sample 16	110±6	16±4	112±37
Sample 17	109±7	18±5	123±37
Sample 19	158±7	10±4	164±44
Sample 20	138±7	16±5	157±42
Average	**131.09±18.24**	**16±3.06**	**131.72±22.88**

TABLE 4:LABORATORY TO FIELD RATIOS.

Sample code	Uranium	Thorium	Potassium
Gap 1	INACCESSIBLE AREA		
Gap 2	INACCESSIBLE AREA		
Gap 3	INACCESSIBLE AREA		
Sample 6	***2.41***	***1.15***	***1.98***
Sample 7	1.87	1.39	1.55
Sample 8	2.06	0.78	1.47
Sample 9	2.61	1.08	2.65
Sample10	2.77	1.17	2.68
Sample 13	2.34	1.18	1.59
Sample 14	1.50	1.34	1.75
Sample 16	1.39	0.88	1.78
Sample 17	2.44	1.05	1.99
Sample 19	1.89	1.64	1.29
Sample 20	1.90	0.92	1.29
Average	2.11 ± 0.42	1.14 ± 0.24	1.82 ± 0.46

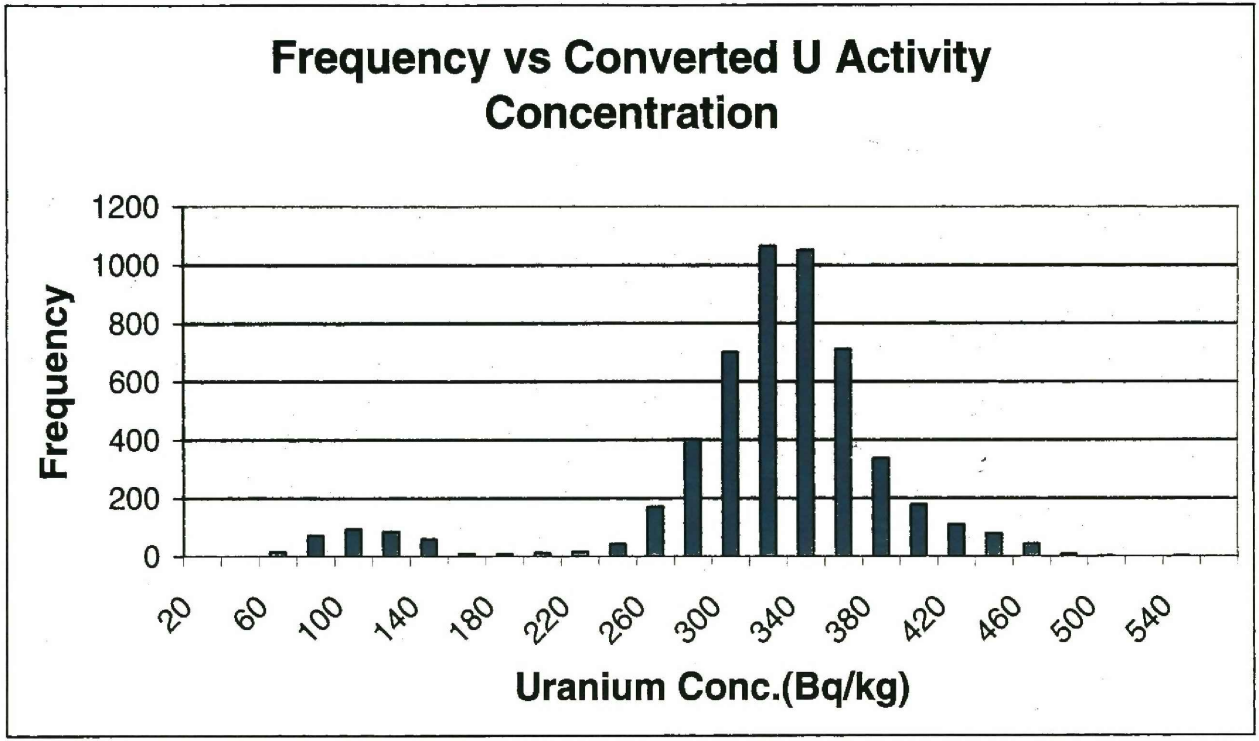

FIGURE 27:A HISTOGRAM SHOWING THE FREQUENCY OF THE URANIUM ACTIVITY CONCENTRATION IN THE FIELD AFTER CONVERSION.

TABLE 14:FREQUENCY DISTRIBUTION OF THE CORRECTED URANIUM CONCENTRATION IN THE FIELD. ***The correction was done using a factor of 2.41.***

U concentration ($Bq.kg^{-1}$)	**Frequency**
20	0
40	0
60	15
80	71
100	93
120	84
140	59
160	10
180	9
200	12
220	17
240	42
260	170
280	402
300	700
320	1066
340	1051
360	711
380	337
400	178
420	109
440	78
460	43
480	8
500	2
520	0
540	2
560	0
Average = 308.73 ± 68.28	

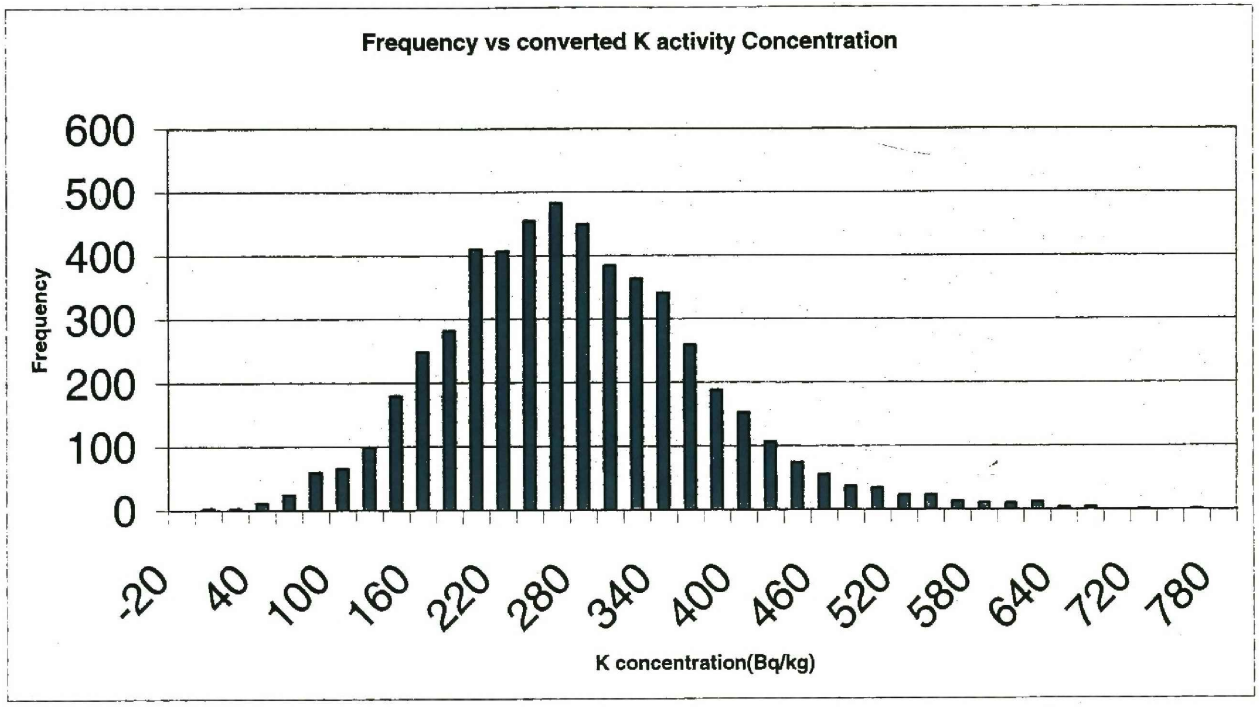

FIGURE 28:A HISTOGRAM SHOWING THE FREQUENCY DISTRIBUTION OF THE POTASSIUM ACTIVITY CONCENTRATION IN THE FIELD AFTER CONVERSION.

TABLE 5:FREQUENCY DISTRIBUTION OF THE CORRECTED POTASSIUM CONCENTRATION IN THE FIELD. *The correction was done using a factor of 1.15.*

K activity concentration. ($Bq.kg^{-1}$)	**Frequency**
-20	0
0	3
20	3
40	11
60	24
80	59
100	65
120	99
140	179
160	248
180	282
200	410
220	407
240	454
260	482
280	449
300	384
320	363
340	341
360	259
380	187
400	152
420	106
440	74
460	55
480	37

500	34
520	23
540	23
560	13
580	11
600	10
620	12
640	4
680	4
700	0
720	1
740	0
760	1
780	0
Average = 264.24 ± 96.55	

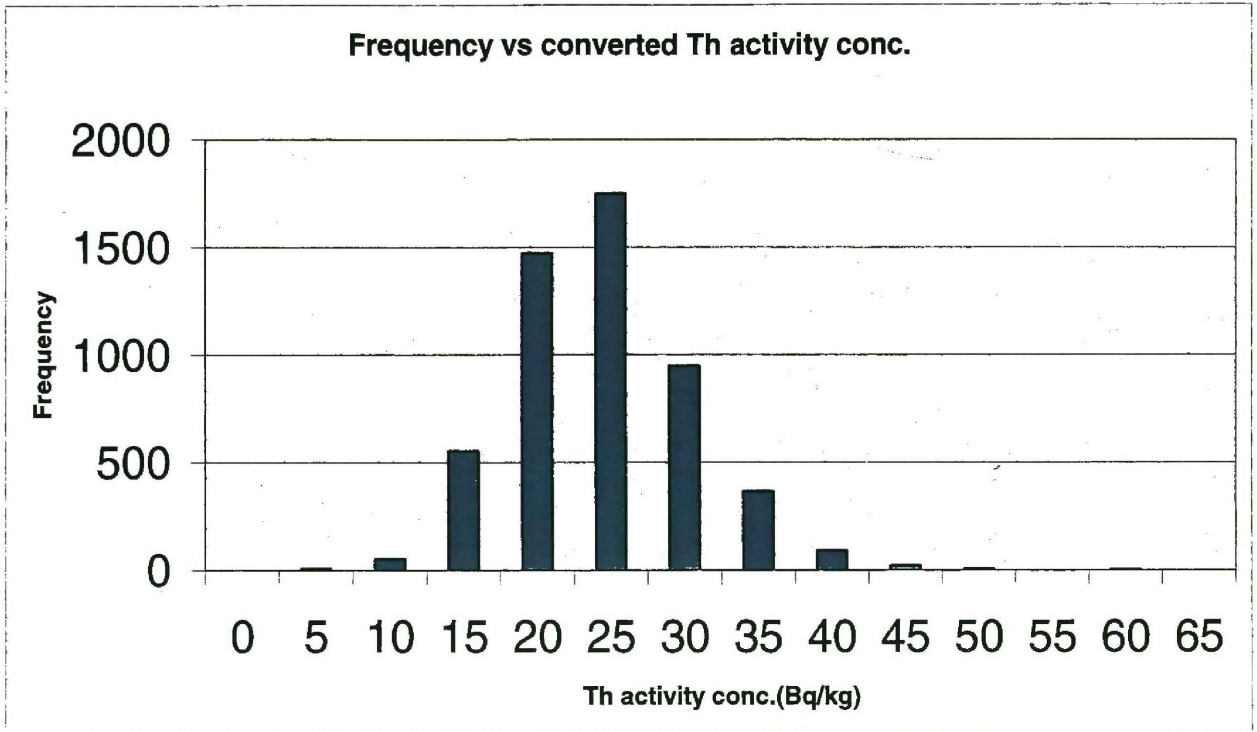

FIGURE 29:FREQUENCY DISTRIBUTION OF THE CONVERTED THORIUM ACTIVITY CONCENTRATION IN THE FIELD.

TABLE 6:FREQUENCY DISTRIBUTION OF THE CORRECTED THORIUM CONCENTRATION IN THE FIELD. *The correction was done using a factor of 1.98*

K Activity concentration ($Bq.Kg^{-1}$)	Frequency
0	0
5	7
10	52
15	553
20	1473
25	1747
30	947
35	366
40	91
45	21
50	8
55	0
60	4
65	0
Average = 21.87 ± 6.03	

6.5 Calculation of radon flux

An equation derived by De Meijer and Lindsay was used to find the radon flux. The derivation of this equation is described in detail in the appendix [6,14]. The equation takes into account several assumptions, which are that:

- The diffusion length is 1metre
- Radium in the field is in secular equilibrium with ^{238}U, as a result, the activity concentration of radium is the same as that of Uranium.
- The longest measured point (sample 6) gave the most correct value to be used for calculation of the conversion factor
- The value for α, is 0.12

$$J = \alpha l \, Cs \, \rho_b \qquad \ldots 6.5$$

Where,

J, *is the flux in* $Bq.m^{-2}.s^{-1}$

α, *Fraction of radon atoms entering going into pore space, dimensionless*

l , *diffusion length of Radon in Soil, in metres(m)estimated to be 1 metre* [12]

λ, *Radon decay constant, which is calculated as ln2/(3.84 x 24 hours x3600 seconds)* $= 2.1x10^{-6}$ *s.*

Cs, Radium activity concentration in the field , $Bq.kg^{-1}$

ρ, *Bulk density of the soil in* $kg.m^{-3}$.

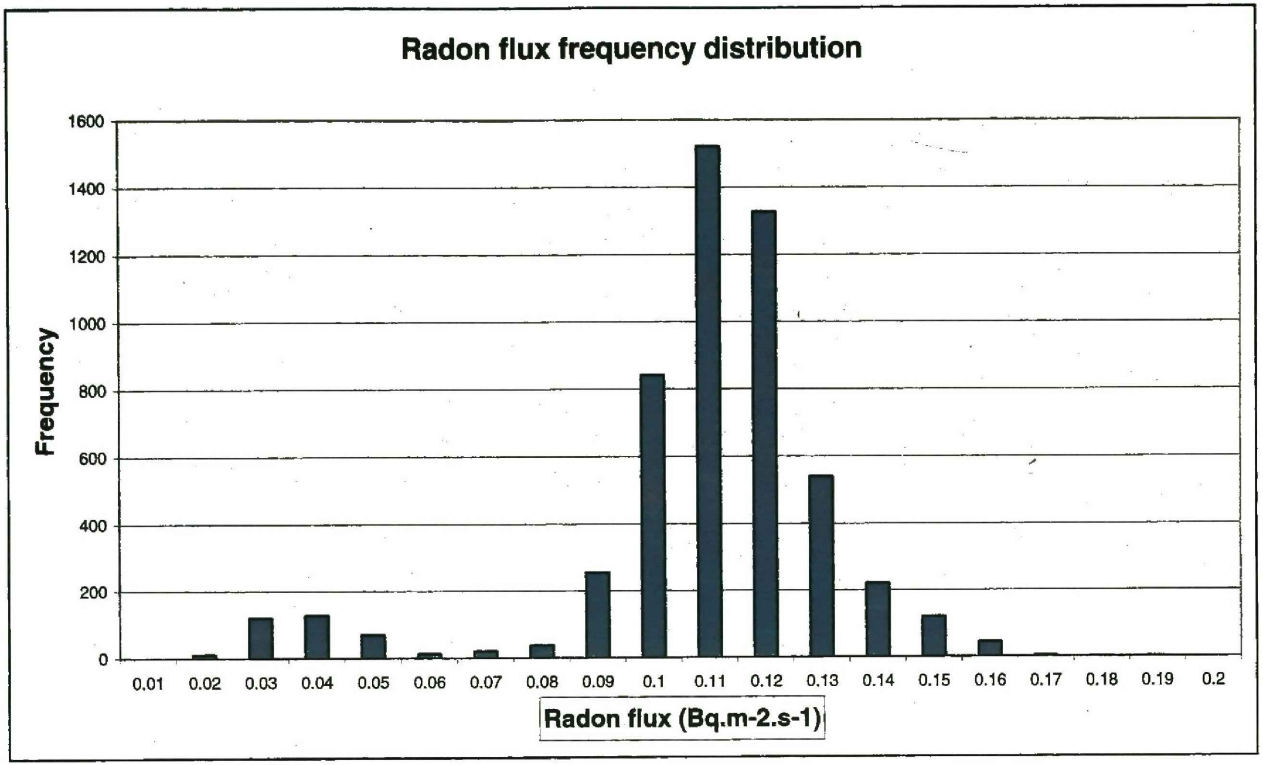

FIGURE 30: A REPRESENTATION OF THE RADON FLUX FREQUENCY DISTRIBUTION IN THE FIELD.

TABLE 7:FREQUENCY DISTRIBUTION OF THE RADON FLUX IN THE FIELD.

Flux ($Bq.m^{-2}.s^{-1}$)	Frequency
0	0
0.01	0
0.02	11
0.03	120
0.04	128
0.05	69
0.06	12
0.07	20
0.08	37
0.09	254
0.1	841
0.11	1521
0.12	1326
0.13	540
0.14	221
0.15	120
0.16	44
0.17	3
0.18	1
0.19	1
0.2	0
Average = 0.105 ± 0.023	

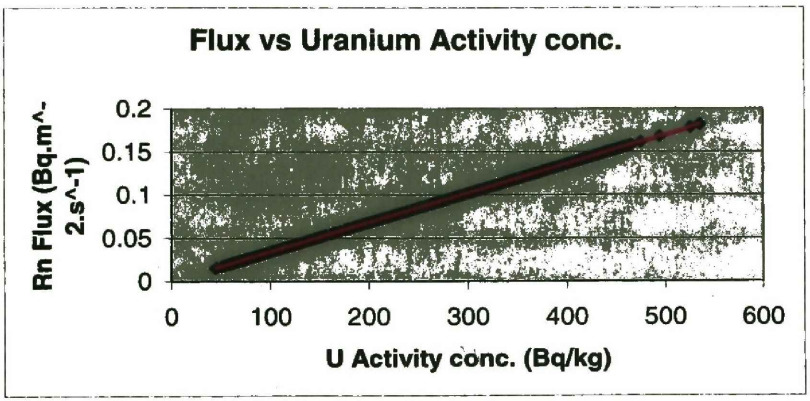

FIGURE 31: RELATIONSHIP BETWEEN URANIUM ACTIVITY CONCENTRATION IN THE FIELD AND THE RADON FLUX.

6.6 Discussion of results

6.6.1 Field results

The data acquired on the field shows that the average Uranium activity for all data points i.e. before being converted to its real value is 128.01± 28.31 $Bq.kg^{-1}$ .The range for this data is 20 –280 $Bq.kg^{-1}$.

Laboratory measurements were used to determine a factor that was used to correct field results to the absolute value. The values after correction gave the mean of the Uranium activity, as 308.73 ± 68.28 $Bq.kg^{-1}$.The range for the data is 60-540 $Bq.kg^{-1}$. The result for individual selected sample points ranges from 109 –166 $Bq.kg^{-1}$ for Uranium, 10 –20 $Bq.kg^{-1}$ for Thorium and 99 –164 $Bq.kg^{-1}$ for Potassium before correction. After being corrected the range for Uranium is 262.9 – 400.4 $Bq.kg^{-1}$.

The equation derived by Lindsay and de Meijer was used to calculate the radon flux with the several assumptions made (see section 6.5). This flux has a mean of 0.105

± 0.023 $Bq.m^{-2}.s^{-1}$. The flux data ranges from 0.02 – 0.19 $Bq.m^{-2}.s^{-1}$ .The relationships between the radon flux and the radium concentration is linear, when the radium activity increases, so does the radon flux. In general, the Uranium/Radium series activity is in the same range as the Potassium while the Thorium is the lowest.

6.6.2 Laboratory results

The laboratory results in general are higher than the field results. This is because in the field, the detector averages activity over a large area while in the laboratory; an individual sample is being measured on a smaller scale and over a longer time.

6.6.3 Comparison to Previous results

A radon flux measurement was done before on the same tailings dam that this research study was carried upon by Sakitha Manatunge in 2001[16]. He was using the passive and dynamic electret systems. His measurements revealed that the radon flux was 0.124 ± 0.046 $Bq.m^{-2}.s^{-1}$ from dynamic system and 0.090 ± 0.077 $Bq.m^{-2}.s^{-1}$ from the passive system . The MEDUSA results is between the two above at 0.105 ± 0.023 $Bq.m^{-2}.s^{-1}$ .The measurements of radon flux done by Kloof mine using diffusion tubes in 1997 on the same tailings dam are tabulated below.See table 17. MEDUSA results are within the previous measurement range but have better statistics than other measurements.

TABLE 8:RESULTS FROM THE DIFFUSION TUBES [23]

	Edge Rn Flux ($Bq.m^{-2}.s^{-1}$)	Beach Rn Flux ($Bq.m^{-2}.s^{-1}$)	Pond Rn Flux ($Bq.m^{-2}.s^{-1}$)
Min	0.003	0.012	0.010
Max	0.844	0.225	0.133
Ave	0.125	0.088	0.058
1SD	0.069	0.029	0.015
2SD	0.139	0.059	0.029

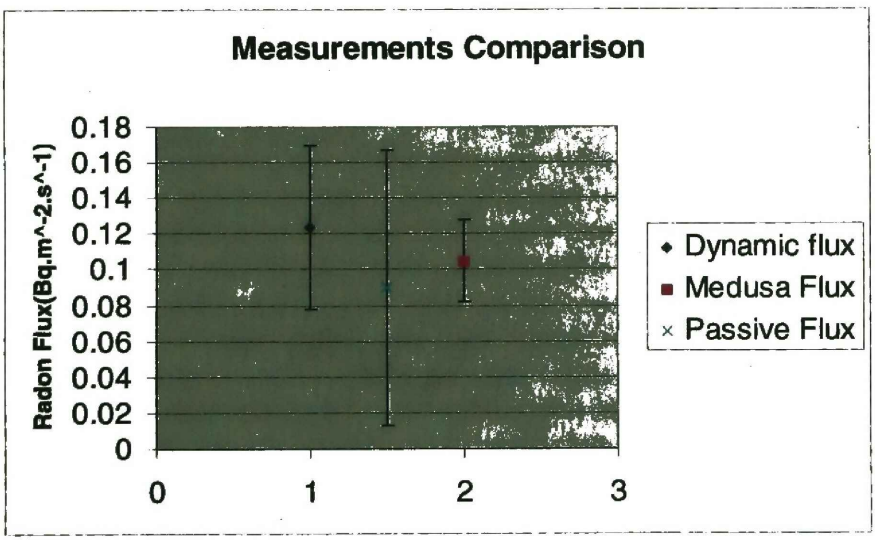

FIGURE 32:COMPARISON OF THE VARIOUS RESULTS ON A MINE TAILINGS DAM.

6.6.5 Theoretical results

Theoretical result was obtained using the following equation as described by IAEA [9].

$$F_t = R\rho E(\lambda D)^{1/2} \qquad ...6.6$$

Where

F_t, *Flux on a given tailings, Bq.kg.m^{-2}.s^{-1}*

R, *Radium concentration, Bq.kg^{-1}(from the converted result as* 308 ± 68.28)

ρ, *Material bulk density, kg.m^{-3}(measured as 1300)*

E, *Emanation coefficient, dimensionless (taken as 3.5,a typical value for South African tailings dams.* [24])

λ, *Radon decay constant,s^{-1}(2.1 x10^{-6})*

D, *diffusion coefficient, m2.s^{-1} (4.215x10^{-7},previously measured.* [26])

The flux obtained ranges from 0.103 – 0.161 Bq.kg.m^{-2}.s^{-1}.This is in the same range as the value estimated in this study.

Chapter 7

Conclusions and recommendations

7.1 Introduction

This chapter summarizes conclusions of the research study and recommends what could be done for the future.

7.2 Conclusions

The main aim of this study was to assess the MEDUSA gamma ray detection system as a tool for measuring radon production on tailings dams. This was done through using the MEDUSA detector on Kloof Gold mine's tailings dam number one. A radioactivity map was produced. This map showed the concentration distributions of Uranium, Thorium and Potassium at various points of the tailings dam where the detector was used. Laboratory measurements were then performed using a Hyper Pure Germanium detector. These measurements enabled a determination of a factor that normalized the field measurements. This factor was found to be 2.4 and it was based on appropriate sampling for a point in the field that was measured for longer than other points, which were measured for one second while driving.

This conversion factor is a function of, the Medusa detector geometry, the sample preparation for the iThemba Environmental Radioactivity Laboratory, ERL, measurements, the Medusa analysis (in particular the standard and background spectra) and the ERL data analysis. If these are kept fixed for future measurements then the factor could be the same for future MEDUSA measurements.

The average radon flux was found to be 0.105 ± 0.023 $Bq.m^{-2}.s^{-1}$. The radon flux ranged from 0.02-0.19 $Bq.m^{-2}.s^{-1}$.

7.2.1 MEDUSA Detector

The MEDUSA detector system is not different in principle to the in situ detectors that have been used before to measure radioactivity. However Medusa has the following advantages,

- It has a highly efficient crystal, which resulted in the measurement of natural radioactivity being achieved in a shorter time.
- The system has software, which uses full spectrum analysis. In full spectrum analysis the entire measured spectrum is fitted to the standard spectra and a background spectrum. This gives a good representation of the activity in the soil, even at short counting times. This together with the efficient crystal makes the detector system unique.
- The system having the above two advantages results in fast analysis. This means that the experiment can be steered according to the user's needs or time constraints.

From the above advantages and the results achieved from the study, the following conclusions are drawn:

- Acknowledging the assumptions made in the equation for calculating flux, the average flux of the tailings area surveyed was estimated to be 0.105 ± 0.023 $Bq.m^{-2}.s^{-1}$. The flux estimated may be taken as the relative flux, until more measurements are done to ascertain the correction factor. This flux is in the same range as the flux that has been measured on the same tailings dam using the electret system as well as the diffusion tube method. It is also in the same range as the theoretical result. The

advantage of the MEDUSA detector system is that they have better statistics. The results of flux are also in the same range as the theoretical results.

- MEDUSA detector system can measure radioactivity concentrations therefore it can be adapted to measure radon flux.
- It has been shown that the radon flux can be estimated based on the MEDUSA results.
- It has been shown that the MEDUSA technique is able to sample the entire tailings dam over a short duration and hence giving a representative sample of the entire tailings dam. It is able to show how non-uniform the flux is across the entire tailings. In this way it addresses the issue of spatial variation. (See the radioactivity maps as well as the tailings dam map on Figure 2)
- The entire tailings dam survey was performed over two days. This was possible due to the detector crystal as well as the software analysis program used by the system. Therefore MEDUSA detector system can cover big space in short time.

7.3 Recommendations

- More tailings dams should be surveyed to establish a generic flux to be used for South African tailings dams i.e. the factor should not just be based on one tailings dam.
- MEDUSA can measure radioactivity, therefore it may also be used in the cleanup or remediation of radioactively contaminated sites.

7.4 Further work

- There should be a detailed calibration of the MEDUSA technique for measurements on tailings dams.
- Accurate measurement of the other factors that are used in the equation for calculating radon flux
- Use of MEDUSA to estimate the radioactivity concentration distribution across a tailings dam.

APPENDIX I

EXHALATION OF RADON FROM A MINE TAILINGS DAM BY MEASURING THE GAMMA RADIATION FROM THE DUMP. [6;14].

Consider a semi-infinite homogeneous layer of consolidated dry sand. The sand with specific density of ρ_s *(which can be approximated fairly accurately by density of sand made of SiO_2 that equals 2.6 g/cm $^{3)}$)* contains C_s Bq/kg of ^{238}U *(as measured in the HPGe at Ithemba LABS)* which is in secular equilibrium with ^{226}Ra, a fraction ε per unit volume is filled with air, (*porosity ε*), hence the grains occupy $(1 - \varepsilon)$ of the volume. Ignoring the mass of the air, the bulk density of the layer is given by:

$$\rho_b = (1 - \varepsilon)\,\rho_s \qquad \text{.....1}$$

For every m^3 of layer, $C_s\,\rho_b$ Bq of ^{226}Ra is present. (ρ_b *measured at UWC based on the mass of material from the tailings*). Due to nuclear decay, ^{226}Ra will turn into ^{222}Rn.A fraction α will leave the grains and enter the air filled void space. Since each Bq of ^{226}Ra produces one radon atom per second, the number of radon atoms entering the void space per second per m^3 equals

$$N_{Rn} = \alpha\, C_s \rho_b \qquad \text{.....2}$$

In secular equilibrium, the total number of radon atoms in the pore space per m^3 of layer follows from the condition that production equals decay:

$$\alpha\, C_s \rho_b = \lambda_{Rn} N = A^{air}_{Rn} \text{ per } m^3 \text{ of layer} \qquad \text{.....3}$$

The activity concentration of Rn in the air-filled pore space becomes:

$$C_{Rn(air)} = \frac{\alpha C_s \rho_b}{\varepsilon} \; Bq.m^{-3} \qquad \text{.....4}$$

In the grain filled part of the layer, the radon production is $(1 - \alpha)\, C_s \rho_b$ atoms per second and hence the volumetric concentration becomes:

$$C_{Rn(grain)} = \frac{(1 - \alpha)\, C_s \rho_b}{(1 - \varepsilon)} \; Bq.m^{-3} \qquad \text{.....5}$$

Note: The total radon concentration under secular equilibrium conditions (*only radon is disappearing by nuclear decay)*

$$C_{Rn(total)} = \varepsilon C_{Rn(air)} + (1 - \varepsilon)\, C_{Rn(grain)} = \alpha C_s \rho_b + (1 - \alpha)\, C_s \rho_b = C_s \rho_b$$

as to be expected. So at great depth we know the partitioning between radon in the grains and radon in the pore space.

Near the surface, radon will diffuse to the surface and exhale into the air. We assume that the radon concentration profile for the air-filled pore space can be written as

$$C(z) = C^{\infty}(1 - e^{-z/l}) \qquad \text{.....6}$$

Where C^{∞} is the volumetric concentration of radon in the pore space at large depth and $l=(D/\lambda_{Rn})^{1/2}$ is the diffusion length with D the effective diffusion constant for radon and λ_{Rn} = the radon decay constant.

According to eq. (4):

$$C^{\infty} = \frac{\alpha C_s \rho_b}{\varepsilon} \qquad \text{.....7}$$

The exhalation per unit of surface is often defined as:

$$J = \varepsilon D \frac{\partial C}{\partial z} \text{ at } z = 0$$

$$= \frac{\varepsilon D}{l} C^{\infty} = \frac{\alpha D}{l} C_s \rho_b \qquad \text{.....8}$$

Radon in the soil decays further into the gamma-ray producing nuclei ^{214}Pb and ^{214}Bi Which are assumed to be in equilibrium with respect to each other and to the ^{222}Rn concentration. At depth z, the volumetric concentration of the 214 nuclei follows from the radon concentration in the grains, which is independent of z, and the z dependent radon concentration in the air filled pore space

$$C^{214}(z) = (1 - \varepsilon)\, C_{Rn(grain)} + \varepsilon\, C_{Rn(air)} = (1 - \alpha)\, C_s \rho_b + \alpha C_s \rho_b (1 - e^{-z/l})$$

$$= C_s \rho_b (1 - \alpha e^{-z/l}) \qquad \text{.....9}$$

Consider again a semi-infinite layer of homogeneous material with density, ρ, and activity concentration of C Bq/kg. Assume that per decay the gamma rays are emitted isotropically.

We simplify the picture by assuming that all gamma rays are emitted perpendicular to the surface. On top of the surface we place a detector with surface A_{det} and efficiency 1. The correction for real efficiency is made later.
The amount of gamma rays emitted towards the detector per unit of volume is set to I_o. The value of Io for a layer with thickness dz is given by

$$I_o\, dz = \tfrac{1}{2} C \rho\, dz \qquad \text{.....10}$$

At the detector, due to absorption one has a count rate of

$$I(z)\,dz = A_{det}\, I_o\, e^{-(\mu/\rho)\rho z}\, dz \qquad \text{.....11}$$

Where μ/ρ is the mass-attenuation coefficient and A_{det} and is the area of the detector.

If C(z) is a constant, the number of gamma rays at the detector follows from the integration:

$$I^{tot} = \tfrac{1}{2}\, A_{det}\, C_s \rho_b \int_0^{\infty} e^{-(\mu/\rho)\rho z}\, dz = \tfrac{1}{2}\, A_{det}\, \frac{C_s \rho_b}{\mu} \qquad \text{.....12}$$

This result can be applied to the case for radon. So in the case that no radon escapes from the soil, we may write

$$I^{eq} = 1/2\, A_{det} \frac{C_s \rho_b}{\mu} \qquad \text{...13}$$

In case of radon exhalation by the surface, I_o is no longer a constant and Eq. (10) becomes

$$I_o\, dz = \frac{A_{det}}{2} C(z) \rho\, dz \qquad \text{.....14}$$

Where C(z) is given by eq. 9. This results in

$$I_o(z)dz = = \frac{A_{det}}{2} C_s \rho\, dz\, (1 - \alpha\, e^{-z/l})\, dz \qquad \text{.....15}$$

The total number of gamma counts in the detector then becomes

$$I = \int_0^{\infty} I_o(z)dz = \frac{A_{det}}{2} C_s \rho_b \left[\int_0^{\infty} \left(e^{-(\mu/\rho)\rho z} - \alpha e^{-(\mu+1/l)z} \right) dz \right] \qquad .16$$

$$= I^{eq} \left[1 - \frac{\alpha \mu l}{\mu l + 1} \right]$$

This equation implies that if α is measured in the laboratory, the value of I (and hence the exhalation rate) follows from the ratio I/I^{eq}.

Since I is linearly dependent on the concentration of radium, C_s,

$$\frac{I}{I^{eq}} = \frac{C_{Ra}\,(field)}{C_{Ra}\,(eq)} \qquad .....17$$

Summary

The ratio in equation (17) can be obtained from the laboratory measurement C_{Ra} (eq) and the field measurements (C_{Ra} (field)). The C_{Ra} (eq) values are found from the sample measurements and the ratios of the ^{214}Pb /^{214}Bi value to the K and Th values. The ratio will then give $[1 - \frac{\alpha\mu l}{\mu l + 1}]$ as a function of the position of the mine. α was measured in the laboratory by measuring the radon release of a small amount of sand material in a calibration jar. The value of μ can be accurately found in literature if it is assumed that the sand is mainly SiO_2. Hence a map of the l values on the tailings can be obtained.

References

1. Benke R. R.; Kearfott K. J.; Comparison of in Situ and Laboratory gamma spectroscopy of natural radionuclides In desert soil; Health Physics Society; 73(2): 350-361;1997

2. Contract book of agreement between iThemba LABS and MEDUSA explorations BV concerning the purchase and use of a MEDUSA type detector; March 2002.

3. Debertin K., Helmer R. G.; Gamma and X-ray spectrometry with semiconductor detectors; Elsevier Science Publishers B.V; Amsterdam (1988).

4. De Martino S., Sabbarese C., Monetti G.;Radon emanation and exhalation rates from soils measured with an electrostatic Collector; Applied radiation and Isotopes, Vol. 49,No. 4,1988

5. De Meijer R. J.;Heavy minerals: From 'Edelstein' to Einstein; Environmental Radioactivity Research and Consultancy Group; Groningen; The Netherlands;1997

6. De Meijer R. J.; iThemba LABS; Faure; South Africa; 2002 *(Private Communication)*

7. Environmental Measurements Laboratory; United States Department of Energy; Section 5; Vol. 1; 28th Edition; 1997

8. Gilmore G., Hemingway J.D.; Practical gamma ray spectrometry; John Wiley and Sons; England; 1995.

9. IAEA Technical Series 333; Vienna; 1992

10. Jacobi W.; Lung cancer risk from environmental exposure to radon daughters; ICRP Publication 50; Radiation Protection Dosimetry; Vol. 24,No. ¼;pp 19-22; 1988.

11. Laas A.; Radiation Protection Officer, Kloof Gold mine; September 2002*(Private Communication)*

12. A.H. Leuschner; AEC, seminar on radon exposure in South Africa; Pelindaba; 1987/10/20.

13. Guidelines on the assessment of radiation hazards to members of the public from mining and minerals processing facilities; National Nuclear Regulator; 1997

14. Lindsay R.; iThemba LABS; Faure; South Africa; 2002*(Private Communication)*

15. Maleka P.P.; Calibration of germanium detectors for applications of radiometric methods in South Africa; An MSc. Thesis; 2001

16. Manatunge S.;The impact of atmospheric pathways on public exposure; MSc. Thesis; 2002

17. Mohajane E.P.; Background radioactivity levels in Gauteng Province; An MSc. Thesis; 2001

18. Nagda N. L.; Radon: Prevalence, measurements, health risks and control; ASTM Manual Series: MNL 15; 1995

19. NCRP Report No. 97;Measurement of radon and radon daughters in air; Bethesda, Maryland; November 1988.

20. Newman R. T. ;Ithemba LABS; *Private communication;* Cape Town; 2002,

21. Pulles, Howard, de Lange, Brenk Systemplanung and Senes Consultants Ltd, Methodologies for assessment of radiological exposure and health risk from slimes dams in South Africa – A sensitivity analysis; a proposal, undated

22. O.J. Pule; Background radioactivity levels in North West Province; An MSc. Thesis; 2001

23. Strydom R.; Screening measurements of radon emitting source terms at Kloof Gold mining Co. Ltd; Kloof Gold mine Public Hazard assessment; Vol 7 ;LB/35/6/10/89; 1997

24. Tsela A. S.; R. J. N Brits; A theoretical study of the effect of various parameters on radon exhalation from mine tailings; SARPA Conference; 1998.

25. Tsela A. S. ;Physics of the radon emanation processes; Ph. D. Thesis;1999

26. Tsela A.S.; National Nuclear Regulator; *Private communication;* Centurion, 2003

27. Tsoulfamidis; Measurement and detection of radiation; McGraw Hill Series in Nuclear Engineering; Hemisphere Publishing corporation; USA; 1983

28. United Nations Scientific Committee;Sources and effects of ionising radiation United Nations Scientific Committee on the effects of ionising radiation- UNSCEAR 2000 report to the general assembly-Vol. I: Sources;2000.

29. Van Cleef D. J.; Determination of ^{226}Ra in soil using ^{214}Pb and ^{214}Bi immediately after sampling; Health Physics 67: 288-289; 1994.

30. Venema L. B., De Meijer; Natural Radionuclides as tracers of the dispersal of dredge spoil dumped at sea; Journal of Environmental Radioactivity 55, Elsevier Science Ltd; 2001

Internet

31. www. Kvi.nl/~annrep/ar 1999; article by: R. Feenstra, J. Limburg, A. Middel

32. www.fbr.org/swksweb/radon. Html

33. www.radelec.com/radon_flux.html.,internet, products of radelec.

34. www.epa.gov/radiation/understand/chain.htm

35. www.salan.org/article

36. www.energy.cr.usgs.gov/radon/georadon/3.html